frontiers | Frontiers in Earth Science

REVIEW
published: 02 May 2022
doi: 10.3389/feart.2022.891393

Advance in Numerical Simulation Research of Marine Methane Processes

Sinan Xu[1,2,3], *Zhilei Sun*[2,3]*, *Wei Geng*[2,3], *Hong Cao*[2,3], *Xilin Zhang*[2,3], *Bin Zhai*[2,3] and *Zijun Wu*[1]*

[1]State Key Laboratory of Marine Geology, School of Ocean and Earth Science, Tongji University, Shanghai, China, [2]Laboratory for Marine Geology, Pilot National Laboratory for Marine Science and Technology, Qingdao, China, [3]The Key Laboratory of Gas Hydrate, Ministry of Natural Resources, Qingdao Institute of Marine Geology, Qingdao, China

OPEN ACCESS

Edited by:
Dong Feng,
Shanghai Ocean University, China

Reviewed by:
Hongxiang Guan,
Ocean University of China, China
Yin Xijie,
Third Institute of Oceanography State Oceanic Administration, China

***Correspondence:**
Zhilei Sun
wuzj@tongji.edu.cn
Zijun Wu
zhileisun@yeah.net

Specialty section:
This article was submitted to Marine Geoscience, a section of the journal Frontiers in Earth Science

Received: 07 March 2022
Accepted: 11 April 2022
Published: 02 May 2022

Citation:
Xu S, Sun Z, Geng W, Cao H, Zhang X, Zhai B and Wu Z (2022) Advance in Numerical Simulation Research of Marine Methane Processes. Front. Earth Sci. 10:891393. doi: 10.3389/feart.2022.891393

Understanding the modern marine methane processes, which can profoundly affect global climate and have far-reaching impacts on human living environments, is critical for research on the global carbon cycle. Thus, modeling of marine methane processes has attracted increasing attention due to models can accurately simulate and predict the environmental effects of methane on marine and atmospheric ecosystems. In this study, we review the applications of modeling works to marine methane processes, including methanogenesis in sediments, transport and reaction of methane in sediments and seawater, and marine methane emissions to the atmosphere. Compiled a large database of global methanogenesis rates and methane fluxes to the sulfate-methane transition zone, we estimate that the global methanogenesis budget in marine sediments is ~0.87 Tmol yr^{-1} and global sedimentary dissolved inorganic carbon produced by anaerobic oxidation of methane is ~8.9 Tmol yr^{-1}. In addition, although anaerobic oxidation of methane in sediments and aerobic oxidation of methane in seawater act as primary filters to prevent methane leakage from sediments to the hydrosphere as well as the atmosphere, large masses of methane in extreme seafloor environments (e.g., mud volcanic eruptions and hydrate leakage) can still escape microbial oxidation and leakage to seawater or the atmosphere. There is still a lack of models that simulate methane in these extreme marine environments. Therefore, more modeling works are needed to assess the efficiency of marine ecosystems, including sediments and hydrosphere, in filtering methane in the event of large-scale methane leakage from the seafloor. This study provides an interdisciplinary view of methane processes in marine systems and helps identify future directions in the modeling of methane processes in marine system.

Keywords: marine methane processes, model application, anaerobic oxidation of methane, aerobic oxidation of methane, carbon cycle

1 INTRODUCTION

Methane (CH_4), the most important greenhouse gas after carbon dioxide (CO_2), plays a key role in the Earth's carbon cycle over geological time and ongoing global warming (Solomon et al., 2009; Etminan et al., 2016; Allen et al., 2018; Nisbet et al., 2019; Akam et al., 2020). Oceans constitute the largest carbon reservoir on Earth and cover about 70% of the world's surface area. Approximately 1,000–5,000 Gt of methane is stored in marine sediments, mainly in the form of methane hydrates (Buffett and Archer, 2004; Burwicz et al., 2011). Even 1% of the methane seeping from sediment can increase the amount of methane in seawater and the atmosphere tenfold (Boetius and Wenzhöfer, 2013). Consequently, numerous modeling studies have been conducted to quantify methane processes in marine sediments and seawater. In this study, we review how models describe methane processes in marine systems, including sediments and seawater.

Compared with CO_2, methane has a relatively short mean lifetime (~9 years) and is very close to a steady state (Dlugokencky et al., 2011). The reduction of methane with hydroxyl radicals (OH^-) in the troposphere and stratosphere is a vital process of removing atmospheric methane (Dlugokencky et al., 2011). As a result, methane emissions are rapidly fed back into the global climate. The concentration and increased rate of methane in the atmosphere have reached their highest level since the preindustrial period (Saunois et al., 2016b). According to the mole fraction of methane in the geologic-atmospheric records, approximately 215 Tg $year^{-1}$ of methane was emitted to the atmosphere in the preindustrial era (Lelieveld et al., 2002). Methane emissions are mainly classified as natural (e.g., those formed in wetlands, termites and oceans) and anthropogenic (e.g., those from rice agriculture, biomass burning, domestic sewage, and coal extraction), with the natural source accounting for most methane emissions. In particular, wetlands (e.g., swamps and tundra) are the largest methane emitting regions (~150 Tg $year^{-1}$) (Bousquet et al., 2006). Methane emissions from human activities are also not negligible. From the preindustrial era to the current period, anthropogenic methane emissions have increased significantly, reaching ~503–884 Tg $year^{-1}$ (Bousquet et al., 2006; Dlugokencky et al., 2011; Saunois et al., 2016a). Coal extraction, crushing, and processing produce ~120 Tg $year^{-1}$ of methane emissions (Bousquet et al., 2006). Rice agriculture and biomass burning also contribute ~30 and ~50 Tg $year^{-1}$, respectively (Bousquet et al., 2006). Moreover, human activities can affect natural emissions. For example, human exploitation of marine hydrates might destabilize the methane hydrates in sediments, resulting in substantial methane emissions.

Owing to global warming concerns and the necessity to extract the vast amounts of methane hydrate resources, marine methane processes are drawing growing interest. The scale of leakage from methane hydrate breakdown in marine sediments is large (~20 Tg $year^{-1}$) due to changes in numerous geological and environmental conditions (Dlugokencky et al., 2011; Ruppel and Kessler, 2017). The transport of methane-rich fluids released by methane hydrate destabilization involves numerous biochemical reactions and complex environmental geological changes that profoundly affect the entire marine ecosystem (Regnier et al., 2011). Thus, the research on marine methane processes is significant for the following reasons: 1) Study of the mechanisms of global warming. Although the total amount of methane released into the atmosphere from the oceans is limited compared to emissions from wetlands and other factors (Dlugokencky et al., 2011; Ruppel and Kessler, 2017), marine sediments are the largest methane reservoir on Earth, most of which is in the form of methane hydrates (Burwicz et al., 2011). Therefore, the stability of methane hydrate reservoirs and their impact on global warming are particularly interesting. 2) The demand for exploration and development of methane hydrate resources. In marine system, the migration of methane fluids is closely related to the accumulation of mineral resources, and is directly involved in the formation of minerals (Schulz and Zabel, 2006). For example, the cold seeping fluids on the seafloor are mainly composed of methane, and cold vents are paramount exploration proxies for methane hydrate resources, especially for shallow-surface hydrate resources. Therefore, the search for cold vents formed by methane hydrate decomposition leakage fluids should be identified for exploring shallow-surface hydrate resources. Further, environmental considerations for the later development of hydrate resources include observation and study of leakage mechanism (Schulz and Zabel, 2006). 3) Research on critical scientific questions in the life and Earth sciences. The transport and reaction of fluids from methane hydrate decomposition involving essential biochemical reactions are a key link in the study of carbon cycle (Ruppel and Kessler, 2017). Moreover, a series of chemical interactions based on methane as the energy base is a prerequisite of life on many celestial bodies, including planets and moons, and a relevant direction for astrobiological research (Miller and Smythe, 1970; Jakosky et al., 1995; Pavlov et al., 2003). Therefore, marine methane processes should be observed and studied to better understand critical scientific questions about the oceanic evolution in geological history and the origin and evolution of life, including those on other planets. In addition, marine methane processes are interesting research issues at the intersection of Earth system sciences and life sciences.

Due to differences in the Gibbs free energy of electron acceptors, the methanogenesis process related to organic matter (OM) degradation occurs in deep sediments with anaerobic environments. The produced methane is transported to upper sediment by molecular diffusion and advection (Schulz and Zabel, 2006; Dale et al., 2008c). Although most seawater is oxygenated (Repeta et al., 2016), the methanogenesis process can occur in the microbial digestive tract and release fresh fecal particles into the ocean. In seawater, methane is mainly produced in the mixed layer, where methane concentration can reach ~5 nM (Bastviken et al., 2004) and the maximum methane concentration leads to the "marine methane paradox" (Lenhart et al., 2015). Owing to the difference in methane chemical potential between the atmosphere and seawater (the net particle flux always flows from the higher chemical energy state system to the lower chemical energy state system), methane in supersaturated surface seawater can leak into the atmosphere

(Holmes et al., 2000; Mrazovac et al., 2012). Modeling works are essential for studying the marine methane processes. 1) Modeling can overcome the spatial and temporal limitations of laboratory conditions. 2) Modeling can quantitatively analyze the variation of methane fluxes during each process. 3) Modeling can reasonably verify the accuracy of experimental data (Boudreau, 1997). In addition, the combination of model and measured data provides a more accurate quantification of methane production and consumption in each marine process. Considerable work has been done by scholars to simulate the abovementioned marine methane processes. Reaction-transport model (RTM) is commonly used to simulate the transport of methane in sediments coupled with methanogenesis and anaerobic oxidation of methane (AOM). The transport of methane-rich fluids in seawater involves the effects of ocean currents, water pressure, and temperature, so more complex mathematical models have been constructed to simulate it (Yamazaki et al., 2006).

In this review, we summarize the modeling research on marine methane processes, including methanogenesis and transport and reaction of methane in sediments, the flux of methane leakage at the sediment-seawater interface (SWI), methane processes in seawater, and methane flux from seawater to the atmosphere.

2 METHANE PROCESSES IN SEDIMENTS

The main processes involved with methane in sediments are methanogenesis, methane phase transition, and methane transport-reaction. In this section, we review the application of models to these processes and the key factors influencing these methane processes.

2.1 Methanogenesis in Deep Sediment

Deep anaerobic marine sediments are the world's largest reservoir of methane (~4.55 × 10^5 Tg C), with 90% of the produced methane stored in the continental margins, which are approximately four to eight times larger than the terrestrial surface biosphere and soils (Reeburgh, 2007; Wadham et al., 2012; Chen et al., 2017). Methanogenesis is the major source of methane in sediments and occurs when porewater sulfate (SO_4^{2-}) is depleted (Jørgensen and Kasten, 2006). There are two main methanogenesis processes (Megonigal et al., 2004; Fenchel et al., 2012; Burdige and Komada, 2015) the autotrophic pathway (using carbon dioxide reduction), and the acetoclastic pathway (using acetate). The latter process usually occurs in fresh inland rivers (Blair, 1998; Conrad, 2005). According to carbon isotopic data combined with model simulations, the main methanogenesis process in marine sediments is carbon dioxide reduction (autotrophic pathway) (Burdige et al., 2016), which is expressed as follows:

$$2CH_2O \xrightarrow{+2H_2O} 2CO_2 + 4H_2 \xrightarrow{-2H_2O} CO_2 + CH_4 \quad (1)$$

The reduction of carbon dioxide can be divided into two steps. First, OM is sequentially broken down into smaller molecules, followed by fermentation, which produces hydrogen gas (H_2). Then, the produced H_2 acts as a driving force for methanogenesis via carbon dioxide reduction (Whiticar, 1999). Modeling has been applied to methanogenesis that relies mainly on OM degradation, which is directly or indirectly involved in almost all biochemical reactions in marine sediments (Arndt et al., 2013). Hence, there are two important factors in methanogenesis modeling: 1) OM degradation rate and 2) switching of OM degradation from sulfate reduction to methanogenesis. Three types of models are commonly used to describe OM degradation (Arndt et al., 2013). 1) Discrete model (*G*-model). This type of model divides OM into a finite number of reactivity fractions, each of which is degraded according to its single degradation constants (Jørgensen, 1978). 2) Reactive continuum model (RCM). This type of model describes OM degradation by assuming a continuous distribution of OM reactivity at the SWI. A commonly used RCM is based on the Gamma distribution function (γ-RCM) (Boudreau and Ruddick, 1991). 3) Power model. This model is an empirical model based on a large dataset of global sedimentary OM data (Middelburg, 1989). According to the OM degradation model, the OM degradation rate can be expressed as follows:

$$R_{OM}(t) = \frac{dG_{OM}(t)}{dt} \quad (2)$$

where R_{OM} denotes the OM degradation rate, t denotes time, and $G_{\mathrm{OM}}(t)$ denotes OM content at time t. The sulfate concentration in porewater is an important indicator of the methanogenesis, as it occurs at a lower sulfate concentration (Burdige et al., 2016). A threshold value for a given sulfate concentration (~0.5 mM) is typically used to describe the change in OM degradation switched from sulfate reduction to methanogenesis (Boudreau, 1996; Arndt et al., 2009; Chuang et al., 2019; Dale et al., 2019). The methanogenesis rate (R_{ME}) is expressed as follows:

$$R_{Me} = \frac{1}{2} \cdot f\left(SO_4^{2-}\right) \cdot R_{OM} \quad (3)$$

where 1/2 denotes the ratio between OM consumed and methane produced (**Eq. 1**), and $f(SO_4^{2-})$ is a function representing to the threshold of sulfate concentration, which is expressed as (Boudreau, 1996; Chuang et al., 2019):

$$f\left(SO_4^{2-}\right) = 1 - \frac{\left[SO_4^{2-}\right]}{\left[SO_4^{2-}\right] + K_S} \quad (4)$$

or by the complementary error function (Martens et al., 1998; Dale et al., 2019):

$$f\left(SO_4^{2-}\right) = 0.5 \cdot \mathrm{erfc}\left(\frac{\left[SO_4^{2-}\right] - K_S}{k_{in}}\right) \quad (5)$$

where $[SO_4^{2-}]$ denotes the sulfate concentration, *K*s represents the threshold of the sulfate concentration, and k_{in} in **Eq. 5** is a parameter controlling the steepness of $f(SO_4^{2-})$. Typically, sulfate concentration decreases with depth. Hence, **Eq. 4** is a monotonically increasing function with depth. However, the OM degradation rate **Eq. 2** is a monotonically decreasing

function with depth. As a result, substituting **Eq. 4** into **Eq. 3** cannot strictly guarantee that the methanogenesis rate **Eq. 3** decreases monotonically with depth, especially in the surface sediments where the change in OM degradation rate is extremely high (Middelburg, 1989). Compared with **Eqs 4**, **5** can solve this problem, as the complementary error function is equal to either 1 or 0 ($f(SO_4^{2-}) = 1$, if $[SO_4^{2-}] < Ks$ or $f(SO_4^{2-}) = 0$, if $[SO_4^{2-}] > Ks$).

From the expression of the methanogenesis rate (**Eqs 2**, **3**), the intensity of methanogenesis in sediments is directly related to the OM degradation rate. Hence, factors affecting OM degradation also influence methanogenesis processes. The content of OM and its reactivity are the main factors that affect OM degradation (Arndt et al., 2013). The higher the OM content at the SWI, the higher is the OM content that can reach in the deep sediments and the higher the methanogenesis rate (Burwicz et al., 2011). Interestingly, the higher the OM reactivity, the lower the methanogenesis rate for the same OM content at the SWI. This is because under higher OM reactivity, more active OM is consumed in the upper sediment, and less OM is transferred to the deep sediment for methanogenesis (Meister et al., 2013). The sedimentation rate is also a paramount factor affecting OM degradation and further methanogenesis (Buffett and Archer, 2004; Burwicz et al., 2011). The sedimentation rate is a critical proxy of depositional environments, as its quantity in shelf regions (~0.05 cm $year^{-1}$) is usually greater than that in deep sea regions (<0.001 cm $year^{-1}$) (Tromp et al., 1995; Burwicz et al., 2011). In addition, a higher sedimentation rate is generally coupled with higher OM fluxes and faster burial processes, promoting methanogenesis (Seiter et al., 2004; Meister et al., 2013).

The above shows the main factors affecting methanogenesis in sediments. We collected methanogenesis data from 48 sites around the global ocean and calculated the total methanogenesis rate in sediments by depth integration. We found that the sedimentation rate (w) and depth of sulfate-methane transition zone (SMTZ) have a well linear regression result with the depth-integrated methanogenesis rate, where methanogenesis is positively correlated with the sedimentation rate ($R^2 = 0.71$) and negatively correlated with SMTZ depth ($R^2 = 0.79$) (**Table 1** and **Figure 1**). The positive relationship between depth-integrated methanogenesis rate and OM reactivity is weak ($R^2 = 0.53$). The distribution of OM reactivity in global marine sediments is complex, and no model can constrain global OM reactivity well (Arndt et al., 2013). For example, shelf regions are generally considered to have high OM reactivity due to high OM flux from inland and marine biosphere, but there is also a large amount of terrestrial refractory OM (LaRowe et al., 2020). Given the deeper water depth, OM fluxes and OM reactivity are generally lower in abyssal regions. However, high OM reactivity was found in the eastern costal of equatorial Pacific regions. The main reasons are warmer water temperature, which enhances net primary production in surface seawater, and lower water column oxygen concentration, which inhibits OM degradation in seawater and promotes more active OM that can reach sediments (Arndt et al., 2013). Based on the empirical formula we obtained (**Figure 1**) and the mean depth of SMTZ in different regions (Egger et al., 2018), we estimated that approximately 0.87 Tmol $year^{-1}$ methane is produced in global deep marine sediments and 78% in shelf regions (water depth <200 m) (**Table 3**).

2.2 Methane Phase Transition in Sediments

Methane produced in bottom sediments has three phase states: gaseous, liquid (dissolved in porewater), and solid (methane hydrates) (Jørgensen and Kasten, 2006). The phase of methane in sediments varies with environmental factors, typically the ambient temperature, pressure, and salinity (Buffett and Archer, 2004; Regnier et al., 2011). The saturation concentration of methane (C_{Sa_Me}) in porewater has been extensively studied and can be expressed by a polynomial in temperature, pressure and salinity (**Eq. 6**) (Duan and Weare, 1992).

$$\begin{aligned} C_{Sa\_Me} = {} & 1.437 \times 10^{-7} STP - 4.412 \times 10^{-5} TP - 4.6842 \times 10^{-5} SP \\ & + 4.129 \times 10^{-9} ST + 1.43465 \times 10^{-2} P \\ & - 1.6027 \times 10^{-6} T - 1.2676 \times 10^{-6} S - 4.9581 \times 10^{-4} \end{aligned} \tag{6}$$

where S, T and p denote ambient salinity (−), temperaure (K), and pressure (atm), respectively. This empirical formula is applied to S of 1–35, T of 273.15–290.15 K, and p of 1–30 atm. If the concentration of dissolved methane in porewater is greater than the methane saturation and the ambient pressure and temperature conforms to the conditions for hydrate formation, methane hydrate will form in the sediment. The zone in the sediment where hydrate stability can be preserved is called the gas hydrate stability zone (GHSZ) (Kvenvolden, 1993). The GHSZ depth is mainly determined by the ambient temperature and pressure. The methane phase transitions from liquid + hydrate to liquid + gas below the GHSZ as geothermal temperature increases with depth.

The saturation of free methane in porewater is a key parameter for assessing the state of methane in sediments (Burwicz et al., 2011; Tishchenko et al., 2005). The transition of the methane phase in the GHSZ involves four main processes: methane hydrate formation (gaseous → solid, **Eq. 7**), methane hydrate dissolution (solid → gaseous, **Eq. 8**), free methane gas formation (dissolved → gaseous, **Eq. 9**), and free methane gas dissolution (gaseous → dissolved, **Eq. 10**). The simplest formulation for the above transition is based on a linear dependence (Wallmann et al., 2006a; Burwicz et al., 2011; Regnier et al., 2011), expressed as follows:

$$R_{GH} = k_{GH} \cdot \left(\frac{[CH_4]}{C_S^{diss}} - 1 \right), \; if \; [CH_4] \geq C_S^{diss} \tag{7}$$

$$R_{DGH} = k_{DGH} \cdot \left(1 - \frac{[CH_4]}{C_S^{diss}} \right), \; if \; [CH_4] < C_S^{diss} \tag{8}$$

$$R_{FG} = k_{FG} \cdot \left(\frac{[CH_4]}{C_S^{free}} - 1 \right), \; if \; [CH_4] \geq C_S^{free} \tag{9}$$

$$R_{DFG} = k_{DFG} \cdot \left(1 - \frac{[CH_4]}{C_S^{free}} \right), \; if \; [CH_4] < C_S^{free} \tag{10}$$

TABLE 1 | Summary of methanogenesis model studies. The table reports data on sedimentation rate (w), the depth of SMTZ, OM content at the SWI (G_{OM}), OM apparent reactivity ($\langle k \rangle$) and depth-integrated methanogenesis rate (R_{ME}) at each site.

Site	Location	Model	w(m yr^{-1})	SMTZ(Mbsf)	G_{OM}(wt%)	$\langle k \rangle$(yr^{-1})	R_{ME}(mol m^{-2} yr^{-1})	Preference
summer	Cape	1-G	0.103	0.05	0.71	1	14.6	Martens et al. (1998)
winter	Cape	1-G	0.103	0.14	0.12	0.6	1.45	Martens et al. (1998)
Eckernfoerde	Kiel Bight	1-G	0.006	0.337	0.42	0.019	0.39	Albert et al. (1998)
Eckernfoerde	Kiel Bight	1-G	0.006	0.319	0.42	0.018	0.44	Albert et al. (1998)
Eckernfoerde	Kiel Bight	1-G	0.006	0.324	0.42	0.017	0.45	Albert et al. (1998)
Eckernfoerde	Kiel Bight	1-G	0.006	0.326	0.42	0.015	0.5	Albert et al. (1998)
Eckernfoerde	Kiel Bight	1-G	0.006	0.319	0.42	0.018	0.436	Albert et al. (1998)
Eckernfoerde	Kiel Bight	1-G	0.006	0.307	0.44	0.018	0.471	Albert et al. (1998)
Eckernfoerde	Kiel Bight	1-G	0.006	0.298	0.46	0.018	0.506	Albert et al. (1998)
Eckernfoerde	Kiel Bight	1-G	0.006	0.3	0.18	0.01	0.201	Mogollón et al. (2009)
Opouawe	Opouawe	1-G	0.0016	0.09	1.2	0.0025	0.132	Dale et al. (2010)
M5	Aarhus Bay	1-G	0.002	0.6	1	0.017	0.246	Dale et al. (2008c)
M1	Aarhus Bay	2-G	0.0002	2.1	0.8	0.208	0.001	Dale et al. (2008c)
S3	Canadian	2-G	0.0001	0.08	3.35	0.03	0.0257	Boudreau et al. (1998)
S4	Canadian	2-G	0.0001	0.07	2.3	0.739	0.075	Boudreau et al. (1998)
S5	Canadian	2-G	0.0001	0.1	5	1.5	0.053	Boudreau et al. (1998)
ODP site 1,040	Costa Rica	2-G	0.0001	30	1.2	0.0000002	0.0069	Hensen and Wallmann, (2005)
SL17	Hydrate Ridge	2-G	0.00025	0.06	2.9	0.0275	0.011	Luff et al. (2004)
SO178 3–4 KAL	Okhotsk	2-G	0.0001	500	0.8	0.00001	0.00025	Wallmann et al. (2006a)
LV28 2–4 SL	Okhotsk	2-G	0.0001	400	1.5	0.0001	0.00076	Wallmann et al. (2006a)
SO178 10–6	Okhotsk	2-G	0.00013	10	2	0.0002	0.0025	Wallmann et al. (2006a)
SO178 13–6	Okhotsk	2-G	0.00093	3	2	0.0002	0.0404	Wallmann et al. (2006a)
SO178 29–2	Okhotsk	2-G	0.00115	4	1.8	0.0003	0.0267	Wallmann et al. (2006a)
LV28 20–2	Okhotsk	2-G	0.0009	3	1.8	0.000206	0.013	Wallmann et al. (2006a)
ODP 997	Blake Ridge	2-G	0.00022	22	1	0.000001	0.0108	Wallmann et al. (2006a)
M48-2	Namibian	3-G	0.0034	1.3	1.5	1.08	0.0396	Dale et al. (2009)
ODP 995	Blake Ridge	Power	0.0004	22	2	0.000016	0.0005	Marquardt et al. (2010)
1,041	Costa Rica	Power	0.000131	20	3.5	0.0000043	0.0008	Marquardt et al. (2010)
1,230	Peru	Power	0.001	5	3.1	0.00102	0.0247	Marquardt et al. (2010)
685	Peru	Power	0.000147	8	3	0.0001	0.0164	Marquardt et al. (2010)
1,233	Chile	Power	0.0011	9.2	2.1	0.00042	0.0101	Marquardt et al. (2010)
1,014	California	Power	0.00079	10	5	0.00032	0.00893	Marquardt et al. (2010)
1,084	Namibia	Power	0.00024	2	8	0.0728	0.0563	Marquardt et al. (2010)
1,258	Demerara	RCM	0.000015	400	0.2	0.000002	0.00000281	Arndt et al. (2009)
A3	Arkona Bassin	RCM	0.00074	1.1	4	0.027	0.0431	Mogollón et al. (2011)
A5	Arkona	RCM	0.0022	0.4	6	0.027	0.431	Mogollón et al. (2011)
A7	Arkona	RCM	0.0019	0.6	4.5	0.027	0.152	Mogollón et al. (2011)
U1341	Beringsea	RCM	0.0005	450	1.5	0.0101	0.0000084	Wehrmann et al. (2013)
Pockmark	Eckernf'orde Bay	1-G	0.005	0.2	1.2	0.003	1	Mogollón et al. (2011)
Pockmark	Eckernf'orde Bay	1-G	0.005	0.4	1.2	0.003	0.33	Mogollón et al. (2011)
A-1	Cape	^{14}C	—	—	—	—	17.52	Crill and Martens, (1987)
St B	Eckernf'orde Bay	^{14}C	—	—	—	—	1.28	Treude et al. (2003)
WK	Kiel	^{14}C	—	—	—	—	0.72	Schmaljohann, (1996)
BL	Kiel Harbour	^{14}C	—	—	—	—	0.63	Schmaljohann, (1996)
NS	Skagerrak	^{14}C	—	—	—	—	0.62	Parkes et al. (2007)
S10	Skagerrak	^{14}C	—	—	—	—	0.59	Knab et al. (2008)
S11	Skagerrak	^{14}C	—	—	—	—	0.48	Knab et al. (2008)
A-1	Cape Lookout Bight	^{14}C	—	—	—	—	0.18	Crill and Martens, (1987)

where $[CH_4]$ denotes the methane concentration, C_S^{diss} denotes the solubility of dissolved methane, C_S^{free} denotes the solubility of gaseous methane, and k_{GH}, k_{DGH}, k_{FG}, and k_{DFG} denote the kinetic constants of gas hydrate formation, free methane gas formation, gas hydrate dissolution, and free methane gas dissolution, respectively.

The thickness of the GHSZ is an essential parameter for assessing hydrate resources (Burwicz et al., 2011). In addition, a sufficient methane source (e.g., deeper hydrate reservoirs and methanogenesis (Burdige et al., 2016)), low temperature, and high pressure are keys to methane hydrate reservoir formation. The minimum content of surface OM content for methane hydrate formation is ~1 wt% (Buffett and Archer, 2004). It is difficult to form methane hydrates in regions within water depth of 600 m because of the high ambient temperature in sediments (Buffett and Archer, 2004), and methane hydrates are commonly found within water depth of 1,000–3,000 m with a bottom water temperature of ~2°C (Kvenvolden, 1993). Methane hydrate formation regions can be divided into passive and active

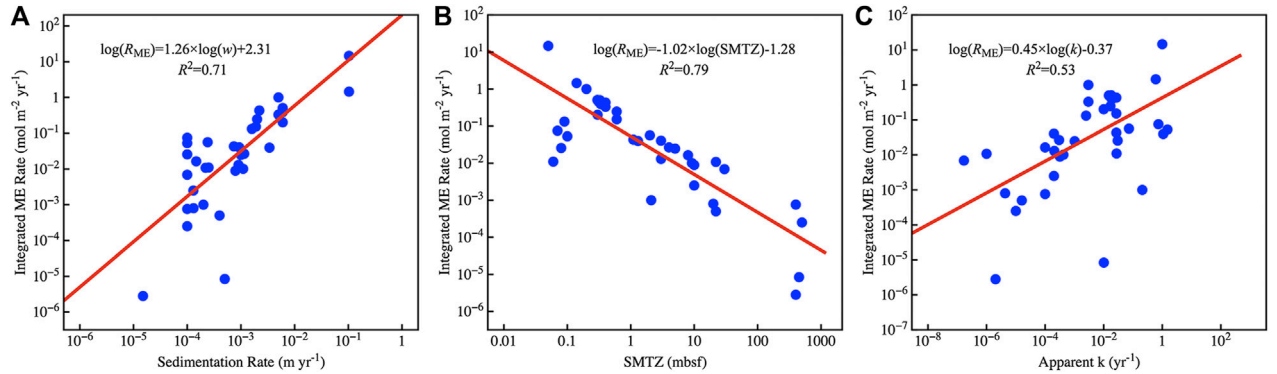

FIGURE 1 | Global empirical relationships. **(A)**. Log–log plots of sedimentation rate and depth-integrated methanogenesis rate. **(B)**. Log–log plots of SMTZ depth and depth-integrated methanogenesis rate. **(C)**. Log–log plots of OM apparent reactivity and depth-integrated methanogenesis rate.

margins (Dale et al., 2008c). Active regions have sufficient overlying methane-rich fluids (methane from deeper hydrate reservoirs), and the abundance of methane hydrates within the GHSZ reaches 30%–50%. By contrast, diffusion dominates the transport of methane in passive margins and hydrate abundances in these regions are smaller (Dale et al., 2008c). The amount of methane stored in marine sediments is within 500–57,000 Gt C (Dickens, 2001; Buffett and Archer, 2004; Milkov, 2004; Klauda and Sandler, 2005; Archer et al., 2009; Burwicz et al., 2011; Pinero et al., 2013; Kretschmer et al., 2015). Buffett and Archer. (2004) first estimated methane hydrate reservoirs in global ocean sediments using the 2-*G* OM degradation model coupled with sulfate reduction, methanogenesis and AOM. They found that the rain rate of particulate OM is key in the global inventory of methane hydrate reservoirs (Archer et al., 2002). In addition, they estimated a total methane hydrate inventory of 3,000 Gt C, but it decreased to 600 Gt C when the methane in the overlying fluid was disregarded (Buffett and Archer, 2004). Klauda and Sandler, (2005) slightly modified Buffett's model and obtained a global methane hydrate inventory of ~57,000 Gt C (Klauda and Sandler, 2005), which was almost two orders of magnitude higher than that of Buffett and Archer. (2004). The main reason for the large error was that the OM degradation model was a 1-*G* model that the entire particulate organic carbon (POC) pool was assumed to be one group with a single degradation rate constant (4.7×10^{-7} year^{-1}). Moreover, biogeochemical reactions associated with the consumption of methane in porewater were ignored (e.g., sulfate reduction and AOM). OM reactivity decreased with sediment depth, whereas this feature cannot be reflected by the *G* model (Middelburg, 1989; Arndt et al., 2013). Burwicz et al. (2011) estimated the global methane hydrate inventory in the range of 4.18–995 Gt C, where the first value refers to present-day conditions (using the relatively low Holocene sedimentation rate) and the second value corresponds to a higher Quaternary sedimentation rate. An RCM (γ-RCM) was used to describe OM degradation in sediments coupled with sulfate reduction and AOM. In addition, an improved power model was used to simulate the OM degradation rate (R_{OM}) (**Eq. 11**) (Wallmann et al., 2006a; Wallmann et al., 2012; Kretschmer et al., 2015).

$$R_{OM}(t) = \frac{K_C}{[DIC] + [CH_4] + K_C} \cdot k_x \cdot G_{OM}(t) \qquad (11)$$

where [DIC] and [CH_4] denote the concentration of ambit dissolved inorganic carbon (DIC) and methane, respectively, K_c denotes the Monod inhibition constant (mM), k_x denotes the age-dependent kinetic constant (year^{-1}), and $G_{OM}(t)$ denotes the OM content. These simulations found that the main factors affecting hydrate storage in the GHSZ were the ambient temperature, oxygen content, sedimentation rate, and upward fluid especially in the active margins (Buffett and Archer, 2004; Burwicz et al., 2011). In particular, ambient temperature is a vital factor influencing the stability of methane hydrate reservoirs, as global methane storage may be reduced by 85% if sedimentary temperature increases by even 3°C (Buffett and Archer, 2004).

According to the global exploration of methane hydrate reservoirs, many sites with hydrates have been discovered globally. **Figure 2** shows the main regions in the world where methane hydrates have been found, such as the Gulf of Mexico (Davidson et al., 1986), Caribbean Sea (Reed et al., 1990), the eastern margin of South America (Jahren et al., 2001), western margin of Africa (Ben-Avraham et al., 2002), Bering Sea (Scholl and Hart, 1993), Sea of Okhotsk (Shoji et al., 2005), Okinawa Trough (Sakai et al., 1990), Sea of Japan (Yun et al., 2011), Shikoku Trough (Saito and Suzuki, 2007), South China Sea (Li et al., 2018), eastern Pacific Ocean (Inagaki et al., 2006), California Coast (Dickens and Quinby-Hunt, 1994), Peruvian margin (Kvenvolden and Kastner, 1990), the Gulf of Oman (White, 1979), Ross Sea and Weddell Sea in the Antarctic (Stoll and Bains, 2003; Giustiniani et al., 2018), and Barents Sea (Andreassen et al., 1990). In addition, the methanogenesis

TABLE 2 | Summary of AOM rate studies. The table reports data on the depth of SMTZ, methane flux into SMTZ (J_{CH}) and depth integrated AOM rate (R_{AOM}) at each site. The check marks indicate the presence of methane hydrates in the bottom sediments.

Site	Location	Water depth(m)	SMTZ(mbsf)	J_{CH}(mol m^{-2} yr^{-1})	R_{AOM}(mol m^{-2} y^{-1})	Hydrates	References
MIC-3	Black Sea	2070	0.02	2.7521	17.2	✓	Wallmann et al. (2006c)
Hydrate Ridge	Cascadia Subduction	775	0.035	5.0808	10.92	✓	Luff et al. (2004)
Hydrate Ridge	Cascadia Subduction	790	0.019	3.69745	10.75	✓	Luff et al. (2005)
MIC-4	Black Sea	2085	0.025	3.4018	10.2	✓	Wallmann et al. (2006c)
Hydrate Ridge	Cascadia Subduction	790	0.025	5.59545	9.25	✓	Luff and Wallmann, (2003)
Hydrate Ridge	Cascadia Subduction	790	0.02	2.8762	9.1	✓	Zeebe, (2007)
MIC-5	Black Sea	2089	0.03	3.27405	6.6	✓	Wallmann et al. (2006c)
Hydrate Ridge	Cascadia Subduction	775	0.05	2.7229	6.09	✓	Luff et al. (2004)
Anaximander	Eastern Mediteranean	1720	0.14	0.04015	6	✓	Haese et al. (2003)
America Trench	Costa Rica Forearc	1,000	0.035	1.59505	5.88	✓	Linke et al. (2005)
Beggiatoa 2	Cascadia Subduction	777	0.05	2.09145	5.62	✓	Treude et al. (2003)
BIGO 4	Cascadia Subduction	778	0.03	3.6938	5.51	✓	Sommer et al. (2006a)
Beggiatoa 1	Cascadia Subduction	777	0.03	3.7157	4.85	✓	Treude et al. (2003)
Hydrate Ridge	Cascadia Subduction	790	0.05	2.77765	4.5	×	Luff et al. (2005)
America Trench	Costa Rica Forearc	1,020	1.4	0.13505	3.5	✓	Schmidt et al. (2005)
Pockmark	Kiel Bight	26	0.05	1.4089	3	×	Albert et al. (1998)
Anaximanders	Eastern Mediteranean		0.25	0.2117	3	✓	Aloisi et al. (2004)
Saanich Inlet	West Coast America	225	0.25	0.22265	2.46	×	Murray et al. (1978)
Hikurangi Margin	New Zealand	700	0.05	3.4748	2.2	✓	Dale et al. (2010)
Saanich Inlet	West Coast America	225	0.12	0.1168	1.4	×	Devol et al. (1984)
Hydrate Ridge	Cascadia Subduction	777	0.125	0.29565	1.31	✓	Sommer et al. (2006a)
Pockmark	Kiel Bight	25	0.09	0.4599	1.1	×	Mogollón et al. (2011)
Saanich Inlet	West Coast America	225	0.18	0.2701	0.955	×	Devol et al. (1984)
Congo Fan	Zaire Shelf	4,000	15.5	0.03285	0.8	×	Zabel and Schulz, (2001)
Eckernfoerde Bay	Kiel Bight	26	0.3	0.2628	0.5	×	Albert et al. (1998)
Green Canyon	Gulf of Mexico	647	3	0.02044	0.5	✓	Ussler and Paull, (2008)
Eckernfoerde Bay	Kiel Bight	26	0.3	0.44165	0.426	×	Martens et al. (1998)
Aarhus Bay (M5)	Baltic Sea	15	0.6	0.0584	0.41	×	Dale et al. (2008b)
Eckernfoerde Bay	Kiel Bight	25	0.29	0.15695	0.39	×	Mogollón et al. (2011)
Eckernfoerde Bay	Kiel Bight	25	0.35	0.09125	0.28	×	Mogollón et al. (2009)
Benguela Coastal	Namibian Shelf	110	1.1	0.03869	0.22	×	Dale et al. (2009)
Cariaco Basin	Venezuelan	40	0.5	0.087965	0.142	×	Reeburgh, (1976)
Amazon Fan	Brazilian Shelf	40	0.7	0.04015	0.1	×	Blair and Aller, (1995)
S10	Norwegian Trench	86	1.3	0.0949	0.09	×	Dale et al. (2008b)
M1	Baltic Sea	27	2.1	0.0657	0.088	×	Dale et al. (2008a)
3,703	Namibian Shelf	1,373	3.5	0.09198	0.08	×	Fossing et al. (2000)
SO178 13–6 KL	Sea of Okhotsk	713	2.7	0.0365	0.0785	✓	Wallmann et al. (2006a)
Site 1,040	Costa Rica Forearc	4,312	3.5	0.0584	0.074	×	Haeckel, (2006)
Aarhus Bay	Baltic Sea	16	1.85	0.00803	0.0621	✓	Thomsen et al. (2001)
SO178 29–2 KL	Sea of Okhotsk	771	3.8	0.025915	0.059	×	Wallmann et al. (2006a)
Amazon Fan	Brazilian Shelf	3,510	4	0.01971	0.055	×	Adler et al. (2000)
3,714	Namibian Shelf	2065	5.8	0.05475	0.055	✓	Fossing et al. (2000)
Sakhalin Island	Sea of Okhotsk	1700	2.5	0.0657	0.049	✓	Aloisi et al. (2004)
LV28 20–2 SL	Sea of Okhotsk	685	2.85	0.004818	0.0454	✓	Wallmann et al. (2006a)
st 4	Black Sea	130	1.8	0.0201,115	0.041	×	Jørgensen et al. (2004)
st 5	Black Sea	181	2.1	0.0190,165	0.035	×	Jørgensen et al. (2004)
S13	Norwegian Trench	361	1	0.1898	0.033	×	Dale et al. (2008b)
Benguela Current	West African Margin	400–2,200	50	0.00073	0.03	×	Sivan et al. (2007)
st 6	Black Sea	396	2.5	0.0217,175	0.03	×	Jørgensen et al. (2004)
st 7	Black Sea	1,176	3.5	0.008103	0.018	×	Jørgensen et al. (2004)
SO178 10–6 SL	Sea of Okhotsk	613	9.8	0.0174,105	0.016	✓	Wallmann et al. (2006a)
ODP997	South-Eastern US	2,770	22	0.0045625	0.0105	✓	Borowski et al. (2000)
Blake Ridge	South-Eastern US	2000–3,000	21	0.00219	0.004	✓	Maher et al. (2006)
ODP leg162 site984A	North Atlantic	1,650	125	0.0000365	0.0031	×	Maher et al. (2006)
LV28 2–4 SL	Sea of Okhotsk	1,265		0.00007665	0.000467	✓	Wallmann et al. (2006a)
SO178 3–4 KAL	Sea of Okhotsk	1,602		0.0000511	0.000205	✓	Wallmann et al. (2006a)
site 1,258	Equatorial Atlantic	2,450–3,200	160–400	0.0002774	0.00003	×	Arndt et al. (2009)
site 1,257	Equatorial Atlantic	3,200	150–400	0.0003869	0.00005	×	Arndt et al. (2006)

model and methane phase transition models were employed to predict the global distribution of methane hydrate reservoirs (Burwicz et al., 2011; Kretschmer et al., 2015). Both exploration and modeling works reveal that methane hydrate reservoirs occur in shallow marine sediments, mainly distributed along the coastal regions of continents (**Figure 2**).

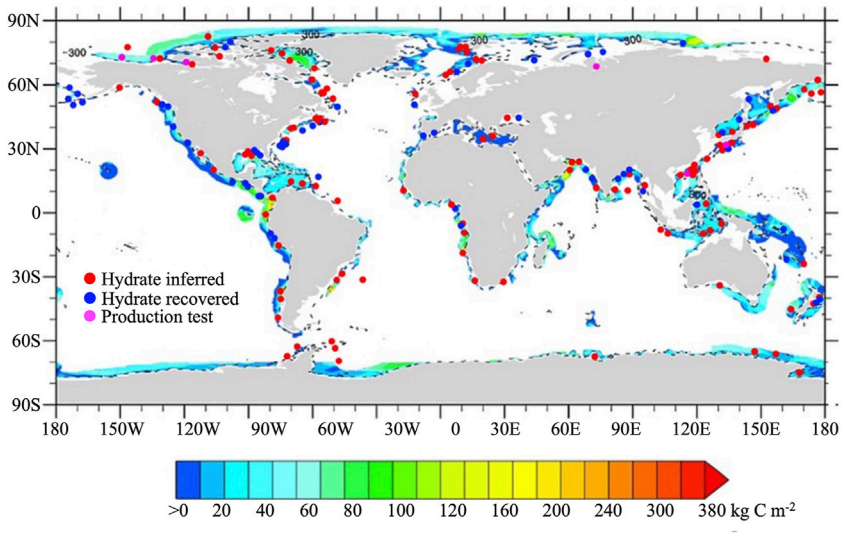

FIGURE 2 | Global distribution of inferred sites, drilling/sampling sites and real production tests for methane hydrate. The underlying map shows global distribution of methane hydrates in marine sediments estimated by model (Kretschmer et al., 2015).

2.3 Transport-Reaction of Methane in Marine Sediments

The methane transported in marine sediments can be divided into dissolved methane (in porewater) and bubbling methane (Regnier et al., 2011). The latter is generated when methane hydrates in the deeper layers break down or when methanogenesis rates are extremely high (Martens and Klump, 1980). Methane transport in the sediment is described by RTM (Meister et al., 2013; Berner, 2020), as follows:

$$\varphi \cdot \frac{\partial [CH_4](x,t)}{\partial t} = \frac{\partial\left(\varphi \cdot \frac{D_m}{\tau^2} \cdot \frac{\partial [CH_4](x,t)}{\partial x}\right)}{\partial x} - \frac{\partial\left(\varphi \cdot w \cdot [CH_4](x,t)\right)}{\partial x} + v \cdot \lambda \cdot \frac{\partial\left([CH_4](x,t) - C_{Sa\_Me}\right)}{\partial x} + \varphi \cdot \sum R(x,t) \tag{12}$$

where x denotes the depth below the seafloor, t denotes time, φ denotes porosity, D_m denotes the molecular diffusion coefficient of methane, τ denotes tortuosity calculated as $\tau^2 = 1 - \ln(\varphi^2)$ (Boudreau, 1997), w denotes the burial velocity, $[CH_4]$ denotes the methane concentration, and R denotes methane related biogeochemical reactions. The methane-rich upward fluid is expressed by the third term on the right side of **Eq. 11**, v denotes the upward fluid velocity, and C_{Sa_Me} denotes the saturation concentration of methane (**Eq. 6**). The parameter $\lambda = 1$, if $[CH_4] > C_{Sa\_Me}$ and $\lambda = 0$, if $[CH_4] < C_{Sa\_Me}$. Methane transport distinctly differs under passive and active conditions. Under passive conditions, the diffusion process dominates the transport of methane on a long-time scale, and methane cannot reach the SWI. By contrast, the advection process under active conditions rapidly pushes the methane from the deeper to the upper sediments within a short time scale (~12 years), and methane can reach the seawater (Dale et al., 2008c).

The most common reaction involved in methane transport is the AOM (**Eq. 13**), which consumes 90% of the methane in the overlying fluids and is thus the biggest methane sink (Reeburgh, 2007).

$$CH_4 + SO_4^{2-} \rightarrow HCO_3^- + HS^- + H_2O \tag{13}$$

From **Eq. 13**, the AOM rate is related to the concentration of methane and sulfate. The simplest model describing the AOM rate is follows (Regnier et al., 2011; Van Cappellen and Gaillard, 1996):

$$R_{AOM} = k_{AOM} \cdot [CH_4] \cdot [SO_4^{2-}] \tag{14}$$

where k_{AOM} denotes the first-order rate constant for the AOM, $[CH_4]$ denotes the methane concentrations, and $[SO_4^{2-}]$ denotes the sulfate concentrations. This model can be easily used to fit measured data and describe the distributions of AOM rates as well as the location and thicknesses of the SMTZs in sediments. In addition, various factors can affect the AOM rate that cannot be reflected by **Eq. 14**, such as temperature, substrate concentration, enzyme reactivity, and bioenergy (Regnier et al., 2005; Dale et al., 2006; Regnier et al., 2011). The concentrations of microorganisms and enzymes involved in the AOM are related to substrate concentration. Specifically, they are limited at low substrate concentrations. In light of this, the AOM rate can be expressed as follows (Regnier et al., 2005):

$$R_{AOM} = v_{max} \cdot \frac{[CH_4]}{[CH_4] + K_m} \cdot \frac{[SO_4^{2-}]}{[SO_4^{2-}] + K_s} \tag{15}$$

where v_{max} denotes the maximum AOM rate, and K_m and K_s represent the half-saturation constants of methane and sulfate, respectively. Furthermore, the minimum energy supply that can facilitate the AOM is ~11 kJ mol^{-1} (Dale et al., 2006), whereas bioenergy available within the SMTZ is limited. Considering the

TABLE 3 | Global budgets of methanogenesis rate and DIC flux related to AOM.

Region (Water Depth (m))	Seafloor Area (km^2)	SMTZ (mbsf)	Me rate (Tmol yr^{-1})	J_{CH} (Tmol yr^{-1})	DIC Flux (Tmol yr^{-1})	Range (Tmol yr^{-1})
Inner shelf (0–10)	2.59×10^6	0.5 (±0.7)	0.28	1.2	2.8	0.5–10.5
Inner shelf (10–50)	9.18×10^6	2.0 (±2.0)	0.24	1.2	2.8	0.5–10.5
Outer shelf (50–200)	1.27×10^7	4.0 (±3.1)	0.16	0.7	1.7	0.3–6.4
Slope (200–2000)	3.01×10^7	12.8 (±12.1)	0.11	0.5	1.3	0.2–4.7
Rise (2000–3,500)	6.28×10^7	143.4 (±222.0)	0.02	0.05	0.15	0.02–0.57
Abyss (>3,500)	2.38×10^8	168.9 (±144.5)	0.06	0.07	0.21	0.03–0.77
Total	3.55×10^8	—	0.87	3.8	8.9	1.55–33.4

The seafloor area data, SMTZ data and methane flux into SMTZ (J_{CH}) data are from Egger et al. (2018). The depth-integrated methanogenesis rate (R_{ME}) were calculated according to the empirical formula in ***Figure 1B****, and DIC flux and its range were calculated according to the empirical formula in* ***Figure 3****.*

limitation of bioenergy, the AOM rate can be expressed as follows:

$$R_{AOM} = v_{max} \cdot F_K \cdot F_T \tag{16}$$

where F_K and F_T denote the kinetic and thermodynamic driving forces for AOM, respectively. The F_K is the abbreviation of the latter two terms of **Eq. 15**, and F_T is expressed as follows:

$$F_T = 1 - \exp\left(\frac{\Delta G_r + \Delta G_{BQ}}{\chi \cdot R \cdot T}\right) \tag{17}$$

where ΔG_r denotes the Gibbs energy of the AOM reaction, ΔG_{BQ} denotes the minimum energy required to sustain the AOM, χ denotes the number of protons translocated across the cell membrane, R denotes the gas constant, and T denotes temperature.

When the methane hydrate in sediments is destabilized or the rate of methanogenesis is high, methane can exist as bubbles in supersaturated porewater (Martens and Klump, 1980). Bubbling methane leakages are widely observed and investigated in coastal sediments (Chanton et al., 1989; Anderson et al., 1998; Veloso-Alarcón et al., 2019). The rate of bubble growth is described by the first-order model (Davie and Buffett, 2001):

$$\Phi = R_b \cdot \left([CH_4] - C_{Sa\_Me}\right) \tag{18}$$

where R_b denotes the rate constant, $[CH_4]$ denotes the methane concentration, and C_{Sa_Me} denotes the saturation concentration of methane in porewater. A continuous three-phase system (solid: hydrate, liquids: porewater, and gas: bubble) has been applied to describe gaseous methane transport in sediments. This approach has been widely applied to soils, aquifers, petroleum and shale gas extraction based on the Darcian flow theory (Schowalter, 1979; Molins and Mayer, 2007; Reagan and Moridis, 2008; Molins et al., 2010). Unlike that of dissolved methane in the porewater, the process of bubble ascent is also influenced by eddy diffusion, which can be described as follows (Haeckel et al., 2007):

$$K_{eddy} \approx 0.928 \cdot \sqrt{g \cdot r_{bubble}^3} \tag{19}$$

where K_{eddy} denotes the first-order eddy diffusivity constant, g denotes the acceleration due to gravity, and r_{bubble} denotes the bubble radius. The velocity of eddy diffusion ($K_{eddy} > 1 \times 10^5$ cm2 $year^{-1}$) is several orders of magnitude greater than that of molecular diffusion, resulting in a sevenfold increase in the maximum AOM rate in the sediments while methane is released into the overlying water column as bubbles (Haeckel et al., 2007). However, the continuous three-phase system assumes that the fluid is transported through a static solid matrix. This limits the application of the system to marine sediments, which are affected by compaction, burial, and particle mixing (Regnier et al., 2011).

Numerous studies have been conducted to simulate AOM reaction in global marine sediments based on **Eqs 12–19** (Regnier et al., 2011). AOM reaction mainly occurs in SMTZ, which is commonly defined as a segment close to the maximum AOM rate. The SMTZ depth varies from 2 cm in the Black Sea (Wallmann et al., 2006b) to 400 m in the equatorial Atlantic (Arndt et al., 2006). Three factors impact the SMTZ depth: 1) methane flux into the SMTZ, 2) upward fluid velocity, and 3) OM content and reactivity (Regnier et al., 2011; Meister et al., 2013; Chuang et al., 2019). Higher methane flux and upward fluid velocity can generate a shallow and narrow SMTZ (Regnier et al., 2011). For example, the SMTZ depth in active margins (~10 m) is much shallower than that in passive margins (~100 m) (Jørgensen and Kasten, 2006; Dale et al., 2008c). Moreover, the higher the content and reactivity of OM in surface sediment, the shallower is the SMTZ, attributable to the consumption of sulfate by OM degradation, which promotes the upward transport of methane-bearing fluids (Meister et al., 2013). The SMTZ is also related to the sedimentation rate. The higher the sedimentation rate, the shallower is the SMTZ (Meister et al., 2013).

The SMTZ acts as the main methane barrier where most electron acceptors are depleted, and OM degradation initiates to dominate methanogenesis (Egger et al., 2018). Approximately ~191 Tmol C $year^{-1}$ of OM is transported to the global seafloor, where 3%–4% of OM is converted into methane (5.7–34.4 Tmol $year^{-1}$) in continental margin sediments (Muller-Karger et al., 2005; Dunne et al., 2007). Egger et al. (2018) compiled methane and sulfate data from 740 sites of global marine sediments and suggested ~3.8 Tmol C annual flux of methane into the SMTZ. According to this methane budget, approximately 3.8 Tmol $year^{-1}$ DIC is produced by the AOM because 1 mol of methane consumed produces 1 mol of DIC (Akam et al., 2020). However, there are some errors in this budget that calculated only by stoichiometric

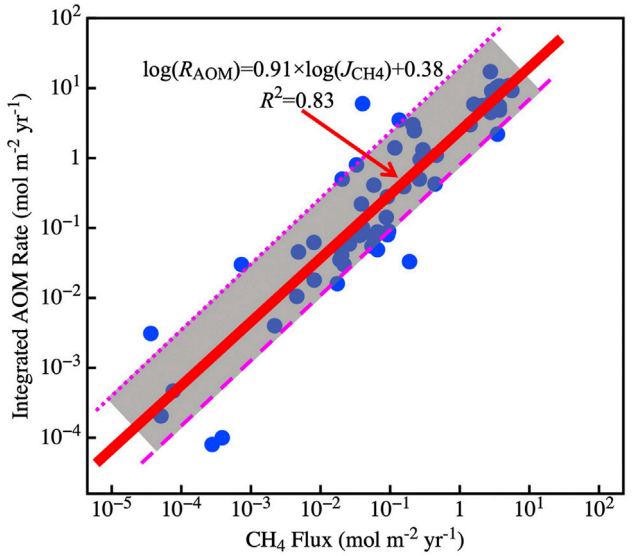

FIGURE 3 | Log–log plots of methane flux into the SMTZ and integrated AOM rate. The gray shaded area indicates the error range of the linear regression, where the upper bound is $\log(R_{AOM}) = 0.91 \times \log(J_{CH4}) + 0.95$, and the lower bound is $\log(R_{AOM}) = 0.91 \times \log(J_{CH4}) - 0.40$.

relationship of the AOM and methane flux data in Egger et al. (2018). The main reason is that the methane flux calculated by Egger et al. (2018) is based on the gradient of methane at locations where porewater methane and sulfate concentrations are equal. However, the flux calculated by Egger et al. (2018) cannot indicate the methane flux involved in the AOM throughout the sediment, and we found that the ratio between this methane flux and depth integrated AOM rate is not 1:1(**Table 2**). Mathematically, the AOM exists throughout sediments, but the concentrations of methane/sulfate in the surface/bottom sediments are too low to detect. Therefore, it is difficult to quantify the total methane flux in the sediments involved in the AOM. Compiled methane flux into the SMTZ data calculated by Egger et al. (2018) and the depth-integrated AOM rate data in the global marine sediments, we found a good regression in the log-log coordinate between the two (**Figure 3**). According to the methane flux distribution in different marine regions and the empirical formula (**Figure 3**), we estimated that ~8.9 Tmol of AOM-related DIC is produced annually, with ~82% being in the continental shelf sediments (water depth <200 m) (**Table 3**).

3 Methane Transport and Reaction in Seawater

Although sediment AOM consumes nearly all upward methane, particularly in passive margins, methane leakages are commonly observed in active margins (Dale et al., 2008d), such as the northern Barents Sea (Andreassen et al., 2017), East Siberian Arctic Shelf (Shakhova et al., 2010), and Gulf of Mexico (MacDonald et al., 1994). The main pathway of methane leakage from sediments to seawater in active margins (e.g., cold seep and pockmarks) is methane plume (Schulz and Zabel, 2006). The formation of authigenic carbonates promoted by AOM processes is an essential factor in the structure of cold seeps and pockmarks (Bohrmann et al., 1998; Luff and Wallmann, 2003; Aloisi et al., 2004; Nöthen and Kasten, 2011).

Cold seeps are often called the "windows to the deep geosphere" (Boetius and Wenzhöfer, 2013), and they form a central link of material and energy exchange between the lithosphere and hydrosphere together with hydrothermal vents systems. Cold seeps formed by hydrate decomposition leakages have globally been found in the entire bathymetric range of the continental slopes from high to low latitudes. For example, more than 1,200 leakages have been detected in the Hornsund Fault Zone of the Barents Sea (Waage et al., 2019), more than 600 leakages have been discovered in the polar North Atlantic (Bear Island Trough, northern Bjørnøyrenna) (Andreassen et al., 2017), approximately 5,000 leakages have been identified in the northern Gulf of Mexico at water depths of >200 m (Solomon et al., 2009), and 27,000 leakages have been detected in the shallow waters of eastern Siberia (Shakhova et al., 2014). Preliminary estimates suggest that there may be over hundreds of thousands of cold-spring leakage sites globally, erupting simultaneously due to hydrate leakage. Large-scale methane leakages on the seafloor are usually caused by the destabilization of hydrate reservoirs located at shallow water depths or buried at shallow depths and connected to fractures (Freire et al., 2011). The following main factors influence these large leaks. 1) Abnormal overpressure. When hydrocarbons accumulate in the pores of marine sediments and the pressure reaches a high enough level, these hydrocarbons will migrate upward through the GHSZ (Tréhu et al., 2004). The decomposition of methane hydrates at the edge of this stability zone can also form a considerable number of hydraulic fractures in its upper part, which then become an ideal channel for gas migration (Xu and Germanovich, 2006). 2) Regional geological environment fluctuation. These changes are observed in seismic activity (Fischer et al., 2013), tidal cycles (Boles et al., 2001), glacial melting (Andreassen et al., 2017), and bottom water temperature fluctuations (Ferré et al., 2020). 3) Erosion of geological bodies. The erosion of the submarine canyons and destabilization of the canyon sidewall sediments lead to the erosion of the hydrate-bearing caps or reservoirs, resulting in the destabilization and decomposition of the hydrate-bearing layers (Paull et al., 2005). 4) Dramatic changes in the global environment. Dramatic global sea level fluctuations and rapid climate warming during geological history could have triggered the catastrophic release of hydrates by disintegration. For example, the amount of methane hydrates that decomposed and escaped to the atmosphere during the Paleocene/Eocene thermal maximum (PETM) was estimated to be ~2,100 Gt C (Dickens et al., 1997).

In the cold seeps, mud volcanoes, or pockmark regions, methane generally seeps into the hydrosphere in the form of gas flares, also called bubble plumes (Boetius and Wenzhöfer, 2013). Only a few *in situ* measurements approaches can be used to calculate methane flux from sediments to the hydrosphere, and they commonly use remotely operated vehicle (ROV). Combined

TABLE 4 | Synthesis of methane flux into hydrosphere and their detection methods.

Site	Location	Water depth(m)	System	Detection method	CH_4 flux	Reference
A	Mediterranean Sea	6,000	mud volcano	ROV (CALMAR)	3 mmol/m^2/d	Caprais et al. (2010)
B	Mediterranean Sea	6,000	mud volcano	ROV (CALMAR)	0.01 mmol/m^2/d	Caprais et al. (2010)
M7	Congo-Angola	3,171	pockmark	ROV (MARUM)	332 mmol/m^2/d	Decker et al. (2012)
M10	Congo-Angola	3,170	pockmark	ROV (MARUM)	492 mmol/m^2/d	Decker et al. (2012)
central dome	Nile Deep Sea	1,250	mud volcano	ROV (QUEST 4000)	1 mmol/m^2/d	Felden et al. (2013)
central dome	Nile Deep Sea	1,250	mud volcano	ROV (QUEST 4001)	24 mmol/m^2/d	Felden et al. (2013)
central dome	Nile Deep Sea	1,250	mud volcano	ROV (QUEST 4002)	70 mmol/m^2/d	Felden et al. (2013)
bacterial mat	Nile Deep Sea	1,250	mud volcano	ROV (QUEST 4003)	49 mmol/m^2/d	Felden et al. (2013)
bacterial mat	Nile Deep Sea	1,250	mud volcano	ROV (QUEST 4004)	83 mmol/m^2/d	Felden et al. (2013)
bacterial mat	Nile Deep Sea	1,250	mud volcano	ROV (QUEST 4005)	85 mmol/m^2/d	Felden et al. (2013)
warm	Svalbard	370	natural seep	Simrad EK60	67 mol/min	Ferré et al. (2020)
cold	Svalbard	370	natural seep	Simrad EK60	38 mol/min	Ferré et al. (2020)
Arcobacter mat	Nile Deep Sea	1,694	pockmark	ROV Victor 6,000	881 mmol/m^2/d	Grünke et al. (2011)
Beggiatoa	Nile Deep Sea	1,120	mud volcano	ROV QUEST 4000	72 mmol/m^2/d	Grünke et al. (2011)
FWCR	South China Sea	1,150	natural seep	GGA	0.12 mmol/m^2/d	Mau et al. (2020)
SSFR	South China Sea	1,150	natural seep	GGA	79.9 mmol/m^2/d	Mau et al. (2020)
SSFR	South China Sea	1,150	natural seep	GGA	3.4 mmol/m^2/d	Mau et al. (2020)
SSFR	South China Sea	1,150	natural seep	GGA	4.8 mmol/m^2/d	Mau et al. (2020)
Clam	N REGAB	3,147–3,165	pockmark	ROV Victor 6,000	1175 mmol/m^2/d	Pop-Ristova et al. (2012)
Clam S	S REGAB	3,147–3,165	pockmark	ROV Victor 6,000	1 mmol/m^2/d	Pop-Ristova et al. (2012)
Clam S Env	S REGAB	3,147–3,165	pockmark	ROV Victor 6,000	3 mmol/m^2/d	Pop-Ristova et al. (2012)
Mussel S	S REGAB	3,147–3,165	pockmark	ROV Victor 6,000	81 mmol/m^2/d	Pop-Ristova et al. (2012)
Mussel S Env	S REGAB	3,147–3,165	pockmark	ROV Victor 6,000	334 mmol/m^2/d	Pop-Ristova et al. (2012)
Clam	SW REGAB	3,147–3,165	pockmark	ROV Victor 6,000	1170 mmol/m^2/d	Pop-Ristova et al. (2012)
Gas	REGAB	3,160	cold seep	ROV Victor 6,000	81 mmol/m^2/d	Pop-Ristova et al. (2012)
Hydrate ridge	Cascadia margin	832	natural seep	BIGO and FLUFO	11.5 mmol/m^2/d	Sommer et al. (2006b)
BIGO 2	Gulf of Cadiz	1,320	mud volcano	BIGO	0.2 mmol/m^2/d	Sommer et al. (2008)
BIGO 1CO	Gulf of Cadiz	1,317	mud volcano	BIGO and FLUFO	0.45 mmol/m^2/d	Sommer et al. (2009)
BIGO 1EX	Gulf of Cadiz	1,317	mud volcano	BIGO and FLUFO	0.08 mmol/m^2/d	Sommer et al. (2009)
BIGO 2EX	Gulf of Cadiz	1,320	mud volcano	BIGO and FLUFO	0.2 mmol/m^2/d	Sommer et al. (2009)
BIGO 4CO	Gulf of Cadiz	1,318	mud volcano	BIGO and FLUFO	0.4 mmol/m^2/d	Sommer et al. (2009)
FLUFO 4BU	Gulf of Cadiz	1,325	mud volcano	BIGO and FLUFO	0.01 mmol/m^2/d	Sommer et al. (2009)
FLUFO 5BU	Gulf of Cadiz	1,318	mud volcano	BIGO and FLUFO	0.04 mmol/m^2/d	Sommer et al. (2009)
FLUFO 5FLUX	Gulf of Cadiz	1,318	mud volcano	BIGO and FLUFO	0.66 mmol/m^2/d	Sommer et al. (2009)
FLUFO-5FLUX	Hikurangi Margin	660	cold seep	MUC and FLUFO	64.6 mmol/m^2/d	Sommer et al. (2010)
FLUFO-1FLUX	Hikurangi Margin	1,098	cold seep	MUC and FLUFO	5.1 mmol/m^2/d	Sommer et al. (2010)
TVG-18	Cascadia margin	650	cold seep	ROV	23 mmol/m^2/d	Suess et al. (1999)
TVG-18	Cascadia margin	650	cold seep	ROV	375 mmol/m^2/d	Suess et al. (1999)
Hydrate ridge	Cascadia margin	778	natural seep	PVC	100 mmol/m^2/d	Torres et al. (2002)
Beggiatoa field (1)	NE Pacific	777	Cold seep	—	0.6 mmol/m^2/d	Treude et al. (2003)
Beggiatoa field (2)	NE Pacific	777	Cold seep	—	4 mmol/m^2/d	Treude et al. (2003)
DMV	Black Sea	2060	Cold seep	ROV	458 mmol/m^2/d	Lichtschlag et al. (2010)
Dnieper delta	Black Sea	240	natural seep	Benthos-300	5.3 mmol/m^2/d	Artemov et al. (2007)
near shore	Belgian zone	200	natural seep	SRI 8610C	0.13 mmol/m^2/d	Borges et al. (2016)
Eckernförde Bay	Baltic Sea	20	pockmark	—	0.07 mmol/m^2/d	Bussmann and Suess, (1998)
Coal Oil Point	California		pockmark	—	68.3 mmol/m^2/d	Hovland et al. (1993)
UK22/4b	North Sea	120	natural seep	—	125 mmol/m^2/d	Leifer and Judd, (2015)
Lookout Bight	United States	30	natural seep	—	3.9 mmol/m^2/d	Martens and Klump, (1984)
Sorokin trough	Black Sea	1,600	mud volcano	ROV	115 mmol/m^2/d	Sahling et al. (2008)
Tommeliten	North Sea	100	natural seep	ROV Cherokee	34.2 mmol/m^2/d	von Deimling et al. (2011)
East Siberian	Arctic Shelf	70	natural seep		4.5 mmol/m^2/d	Shakhova et al. (2014)
Northern US	Atlantic margin	180–600	natural seep	Okeanos Explorer	0.01 mmol/m^2/d	Skarke et al. (2014)
Eckernförde Bay	Baltic Sea	26	pockmark	MBES	1.9 mmol/m^2/d	Lohrberg et al. (2020)
Eckernförde Bay	Baltic Sea	26	pockmark	MBES	3.3 mmol/m^2/d	Lohrberg et al. (2020)
Eckernförde Bay	Baltic Sea	26	pockmark	MBES	0.98 mmol/m^2/d	Lohrberg et al. (2020)
	Mexico Gulf	1,500	natural seep	ROV	160 × 10^3 Mg/yr	Weber et al. (2014)
Makran	Makran margin	575–2,870	natural seep	ROV (QUEST 4004)	1,152 Mg/yr	Bohrmann et al. (1998)
Kerch seep area	Black Sea	890	natural seep	Seal 5,000	11.9 × 10^3 Mg/yr	Römer et al. (2012)
Central Nile	Mediterranean	1,500–1800	natural seep	ROV (QUEST 4004)	0.6 × 10^3 Mg/yr	Römer et al. (2014)
Dutch Dogger	North Sea	45	natural seep	SBES EK60	593 Mg/yr	Römer et al. (2017)
	Mexico Gulf	3,500	natural seep	ROV	9.9 × 10^3 Mg/yr	Römer et al. (2019)
Kerch Peninsula	Black Sea	1,200	natural seep		55.6 × 10^3 Mg/yr	Römer et al. (2020)
	Cascadia margin	920–1,350	natural seep	ROV Doc Ricketts	88 × 10^3 Mg/yr	Riedel et al. (2018)
	Makran Margin	825–2,865	natural seep	Haiyangdizhi 10	5.9 × 10^3 Mg/yr	Wei et al. (2021)

(Continued on following page)

TABLE 4 | (*Continued*) Synthesis of methane flux into hydrosphere and their detection methods.

Site	Location	Water depth(m)	System	Detection method	CH_4 flux	Reference
Candles	Green Canyon	1,170–1,240	natural seep	ROV	8.2×10^5 mol/yr	Johansen et al. (2020)
Mega Plume	Green Canyon	1,170–1,240	natural seep	ROV	5.2×10^6 mol/yr	Johansen et al. (2020)
Haakon Mosby	Barents Sea	1,280	mudvolcano	ROV Victor 6,000	35×10^6 mol/yr	Niemann et al. (2006)
Haakon Mosby	Barents Sea	1,280	mudvolcano	ROV Victor 6,000	40×10^6 mol/yr	Niemann et al. (2006)

with ROV observation, methane flux (F_{methane}) at the SWI can be estimated as follows (Blomberg et al., 2016; Lohrberg et al., 2020; Mau et al., 2020):

$$F_{methane} = N \cdot n_{methane\_bubble} \cdot M_{methane} \cdot f_{methane} \tag{20}$$

where N denotes the number of seep locations, $n_{\text{methane\_bubble}}$ denotes the amount of methane per gas bubble, M_{methane} denotes the molar mass of methane, and f_{methane} denotes the gas bubble emission frequency, which can be obtained by ROV observation. Another method of estimating methane efflux is the box model that the box is defined by the hydrocasts model (Mau et al., 2020), as follows:

$$F_{methane} = \frac{I \cdot u(z) \big/ l_{path}}{A} \tag{21}$$

where I denotes the estimated methane inventory within the box, $u(z)$ denotes the current velocity, l_{path} denotes the migration of the entire box away from its original position, and A denotes the surface area of the grid. In addition, according to porewater methane profiles, methane flux at the SWI can be calculated by Fick's first law (**Eq. 22**) (Haese et al., 2003; Chen et al., 2017), as follows:

$$F_{methane} = \varphi \cdot D_m \cdot \frac{d[CH_4]}{dz} \tag{22}$$

where φ denotes porosity, D_{m} denotes the molecular diffusion coefficient of methane, and the last term represents the gradient of methane concentration at SWI.

We collected methane flux data in cold seep and pockmarks (**Table 4**). The largest methane flux (1,169–1,175 mmol m^{-2} d^{-1}) is at the center of the giant pockmark REGAB located in the West African margin at a water depth of 3,160 m (Pop-Ristova et al., 2012; Boetius and Wenzhöfer, 2013). The regional methane flux can be obtained on the basis of gas flares observed on the seabed and the estimation of the methane flux at each flare. As shown in **Table 4**, 2.5–169.9 Mg $year^{-1}$ of methane flux is identified in the Gulf of Mexico regions (~6,041.25 km^2), of which more than 90% is occupied by the northern Gulf of Mexico (Weber et al., 2014; Römer et al., 2019; Wei et al., 2021).

The transport of methane in seawater, commonly in the form of gas flares or plumes, is an extremely complex process, where bubble plumes are rapidly dissolved and subsequently diluted by mixing with overlying seawater and then dispersed by ocean currents (Graves et al., 2015). The Navier-Stokes equations are commonly used to describe hydrothermal plumes in the seawater where momentum, mass, heat, methane saturation, and microbially-mediated chemical reactions are considered (Yamazaki et al., 2006; Jiang and Breier, 2014). The radius of methane bubbles (R_{bubble}) typically ranges from 0.001 to 0.015 cm (Shakhova et al., 2014; Higgs et al., 2019). The bubbles less than 10 mm in diameter are expected to dissolve before they reach the surface mixing layer (Gentz et al., 2014). The rate of bubble dissolution depends mainly on the initial bubble size, water temperature, salinity, pressure, and bubble rise rate (Leifer and Patro, 2002; Rehder et al., 2009; Shagapov et al., 2017). The bubble dissolution rate can be written as follows (Fu et al., 2021):

$$\frac{dM}{dz} = \frac{-\left(4\pi R_{bubble}^2\right) \cdot K \cdot (C_S - C_0)}{V_{bubble}} \tag{23}$$

where dM/dz denotes the change in a bubble's methane content over the rise interval dz, V_{bubble} denotes the bubble rise velocity, and K denotes the mass transfer rate.

Based on large ROV observations of methane bubble radius (R_{bubble}) and bubble rising velocity (V_{bubble}), empirical formulae were used to describe bubble rise velocity, as follows (Clift et al., 2005; Leifer et al., 2006):

$$V_{bubble} = 276R_{bubble} - 1648R_{bubble}^2 + 4882R_{bubble}^3 - 7429R_{bubble}^4 + 5618R_{bubble}^5 \tag{24}$$

The well-known theory of Morton, Taylor and Turner (MTT model) has been used to estimate the maximum rising height of a single plume (Morton et al., 1956), and the scaling of the maximum plume rise height (Z_{max}) is given as follows:

$$Z_{max} = C_e \cdot \left(\frac{B_{exit}}{N^3}\right)^{\frac{1}{4}} \tag{25}$$

where B_{exit} denotes the source flux, N denotes the ambient frequency, and C_{e} denotes the scaling coefficient, which was estimated to be 3.76 by analyzing literature data from laboratory plume experiments (Briggs, 1969).

Compared with methane reaction in sediments with sulfate (AOM) in anoxic environments, bottom waters in the continental margin are generally completely oxygenated, with oxygen concentrations ranging from 250 to 350 μM (Boetius and Wenzhöfer, 2013). The consumption of methane in the hydrosphere is related to oxygen, as aerobic oxidation of methane (AeOM):

$$CH_4 + O_2 \rightarrow CO_2 + H_2O \tag{26}$$

The AeOM rate can be calculated as follows (Reeburgh et al., 1991; Valentine et al., 2010; Mau et al., 2020):

$$R_{AeOM} = k \cdot [CH_4] \tag{27}$$

where k denotes the first-order rate constant, and $[CH_4]$ denotes the methane concentration. Many factors that influence AeOM, such as (1) water depth; (2) temporal and spatial distributions of fluid release flux; (3) bubble characteristics (e.g., size, oil film and hydrate coating) (Veloso-Alarcón et al., 2019); (4) ocean euphotic layer; (5) dissolved oxygen concentration, temperature and salinity of seawater (Crespo-Medina et al., 2014); and (6) ocean currents (Steinle et al., 2015). According to the data compiled by Boetius and Wenzhöfer, (2013), the contribution of AeOM to methane consumption in seeps regions can exceed the contribution of AOM, particularly at seeps with low microbial abundance. In regions with low methane fluxes, the AOM consumes 90% of the methane in the overlying fluid (Reeburgh, 2007), whereas most of the methane transported to the seafloor in the seepage regions is consumed by the AeOM (Boetius and Wenzhöfer, 2013).

In cold seep regions, the efficiency of the methane filter (AOM and AeOM) decreases from ~80% for low fluid flow systems (methane flux: ~35 mmol m^{-2} d^{-1}) to ~20% for moderate flow systems (methane flux: ~100 mmol m^{-2} d^{-1}). With microorganisms and bacterial mats absent and with intense gas eruptions, the filter efficiency becomes lower than 10% in high fluid flow systems (e.g., giant pockmark systems) (Pop-Ristova et al., 2012; Boetius and Wenzhöfer, 2013). When such a large amount of methane escapes from microbial oxidation on the seafloor, it will be consumed aerobically in the seawater or transferred to the upper mixed layer and then to the atmosphere (Reeburgh, 2007; Boetius and Wenzhöfer, 2013).

4 METHANE FLUX TO THE ATMOSPHERE

Owing to the human activities, the concentration of greenhouse gases in the atmosphere has been increasing since the 20th century, causing global warming (Sommer et al., 2009; Anderson et al., 2016). The greenhouse effect causes some ecological problems such as glacier retreat, sea-level rise, and the northward shift of the climate zone, which will cause great harm to the natural environment (Larcombe et al., 1995). As the main greenhouse gas, it is significant to calculate the amount of methane transported from seawater to the atmosphere.

The methane flux released from seawater to the atmosphere has been mainly predicted by digital simulation and remote sensing technology (Bovensmann et al., 2010). These methods usually use scientific ship positioning measurements and reverse atmospheric models to estimate methane release. For example, during the 2012 North Sea Elgin blowout accident, such a method was used to assess methane emissions to the atmosphere (Gerilowski et al., 2015). Considering this technology is relatively clumsy and inflexible, passive remote sensing techniques have been developed to collect atmospheric methane concentrations around the study areas, such as wireless remote sensing to collect atmospheric methane concentrations around the study region (Somov et al., 2013; van Kessel et al., 2018). However, when surveying with remote sensing instruments using short-wave infrared radiation, the weak reflectivity of water affects the information (Seelig et al., 2008).

The model calculates the methane flux at the sea-air interface mainly based on the differences in methane chemical potential between seawater and the atmosphere (Seelig et al., 2008). When methane is supersaturated in seawater, the methane in seawater can be emitted to the atmosphere driven by chemical potential. The methane fluxes to the atmosphere are calculated by the diffusive exchange equation (Solomon et al., 2009; Michel et al., 2021):

$$Flux_{Methane} = k_{avg} \cdot \left(C_{plume} - C_{eq}\right) \tag{28}$$

where k_{avg} denotes the gas transfer coefficient at the average wind speed, and C_{eq} denotes the seawater methane concentration in equilibrium with air under ambient conditions (Yamamoto et al., 1976). The gas transfer coefficients are calculated using the empirical formula (Wanninkhof, 1992), as follows:

$$k_{avg} = 0.31 \cdot u_{avg} \cdot \left(\frac{S_C}{600}\right)^{-0.5} \tag{29}$$

where u_{avg} denotes the average wind speed at 10 m above the sea surface, and S_c denotes the Schmidt number (a function of salinity and temperature).

The combined cycle model for CO_2 and CH_4 (CMCDMC) was used to assess the role of different environmental parameters in the natural and anthropogenic components of methane leakage and climate change (Krapivin et al., 2017). Given that low-rate methane leaks are nearly completely consumed by the AOM, the climatic impact of methane may be overlooked. However, the high-rate leakage enables methane to enter the seawater and atmosphere directly, thereby causing global warming (Buffett and Archer, 2004). Although there is no conclusive evidence that hydrate-derived methane presently enters the atmosphere, more observational data and improved numerical models will help better describe the climate-hydrate synergy in the future (Ruppel and Kessler, 2017).

5 CHALLENGES AND OUTLOOK

The application of the model to the marine methane processes is summarized as shown in **Figure 4**, including methanogenesis, methane transport and reaction in sediments and seawater, and methane flux from seawater to the atmosphere. The global ocean methane cycle has been increasingly studied, and considerable progress has been made in understanding the marine methane cycle. However, many environmental factors involved in methanogenesis, methane reaction and transport have not been described well by the models. Human understanding of the global methane cycle and the capability to assess the contribution of methane leakage to past and future global changes depend heavily on the accuracy of model construction and calculations. Future progress will rely heavily on additional observational data from different marine environments in the global ocean and on linking models to the observed complexities. Below, we list the remaining problems concerning methane cycle processes to help direct future research.

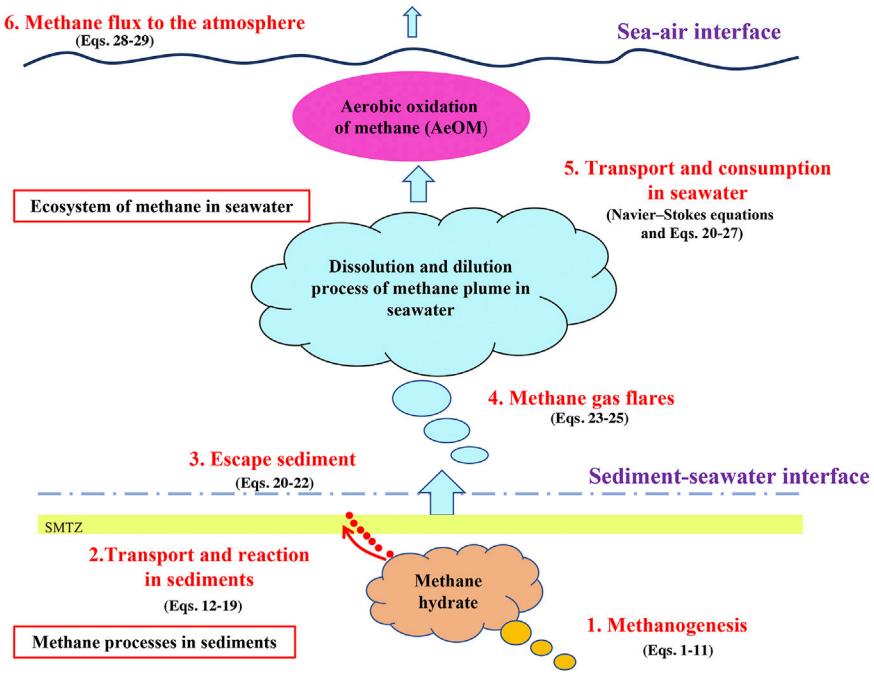

FIGURE 4 | Schematic diagram of the application of model in the marine methane processes.

5.1 Metal-dependent AOM (Metal-AOM)

Sulfate–driven AOM is widely found in global marine sediments, but scholars have found that AOM driven by some active metals (e.g., manganese and iron) is also quite common (Beal et al., 2009). The reduction of the other metal ions with methane is often neglected because the concentration of sulfate in porewater is several orders of magnitude higher than those of other electron acceptors and the almost complete consumption of methane (Reeburgh, 2007). If the manganese flux (~19 Tg year^{-1}) and iron flux (~730 Tg year^{-1}) of the whole world were used to oxidize methane, the result might account for around a fourth of today's AOM consumption. Even if only a small portion of manganese and iron fluxes is used for the AOM, the process can be a massive methane sink, as manganese and iron may be oxidized and reduced by 100–300 times before being buried (Canfield et al., 1993; Beal et al., 2009). Although several experimental studies have been conducted on metal-AOM (Sivan et al., 2011; Egger et al., 2015; Ettwig et al., 2016), there is no single study that assesses metal-AOM via a modelling approach. Thus, more modelling work about metal–AOM needs to be done to help quantify global metal-AOM and enhance the understanding of the changes of δ^{13}C-DIC in porewater.

5.2 Model Construction, Boundary Conditions, and Marine Biological Environments

As methane plumes mainly originate from the decomposition of methane hydrates, transport to the seawater, and eventually reach the atmosphere, a continuum model should be established to describe methane transport in different media (sediment, seawater and atmosphere). At present, the boundary conditions, the initial conditions, and parameters of the mathematical models used for marine geological investigations are ideal (Boudreau, 1997). The transport of porewater species and the initial and boundary conditions are always set as a constant or closed boundary. Further, the pressure and temperature boundary conditions given for simulating the decomposition and release of methane from seabed natural gas hydrates are within a limited predicted range. For complex geological processes, the selection of boundary conditions should be closely combined with field monitoring or laboratory experimental data rather than a simple boundary prediction range or constant. The boundary conditions for methane leakage from sediments and methane migration through different media should be a set of complexes, dynamic boundary conditions that biochemical and geological factors should be considered.

Methane transport in the seabed and seawater is affected by marine and geological organisms (Keppler et al., 2009). Therefore, model accuracy and sensitivity are strongly related to the consideration of biological factors. At present, most mathematical models are lacking in accounting for the effects of marine organisms on methane transport, or the effects of these marine biological factors are treated as a constant (Chuang et al., 2019). By contrast, the activity of marine organisms is influenced by multiple factors. Thus, further work is needed to describe the impact of marine organisms on the methane cycle. The results of field investigation and experimental analyses of recent biochemical reactions of methane should be employed to characterize the models.

5.3 Methane Leakage on the Seafloor

Hydrate can be formed when the seabed temperature and pressure reach certain conditions and if there is a leak that adds alkane fluids to the seabed. Therefore, the stable boundary of hydrates may be at a certain depth in the water body, and the reservoir location may not necessarily be in the sediment. The Gulf of Mexico (Brooks et al., 1994; Boswell, 2009), Joetsu basin in Japan, and the South China Sea have exposed hydrate outcrops or shallow hydrates on the seafloor (Hiruta et al., 2009; Zhang et al., 2017). When methane bubbles ascend on the seafloor in some areas, their surfaces can rapidly form hydrate crusts during upward migration. Therefore, the bubble plumes at the leakage point of cold seeps can be classified as "clean" or "dirty" (Barnes and Goldberg, 1976). There is no numerical simulation for bubble leakage under these conditions. For some anoxic "euxinic basins," such as Cariaco Basin and Black Sea (Reeburgh et al., 1991; Van Rensbergen et al., 2002), research on the processes of methane transport also lacks simulation. Therefore, there is a large room for improvement in accurately simulating modern seabed methane processes, especially methane leaks associated with gas hydrates.

5.4 Predictive Capability of Accidental Large-Scale Methane Leakage

The major advantage of the modeling approach is that it can reasonably predict the trend of methane transport under predetermined conditions (Boudreau, 1997). Owing to the AOM process, methane in sediments hardly seeps into the seawater, or it seeps into the seawater only for a short period (<60 years) and is then quickly re-limited in sediments by the AOM process (Dale et al., 2008c; Regnier et al., 2011). Many ROV observations reveal that strong gas ebullition in the cold seeps or mud volcano regions allows a massive amount of methane to escape microbial oxidation in sediments and be ultimately transported to seawater or even the atmosphere (Boetius and Wenzhöfer, 2013; Andreassen et al., 2017). Nevertheless, there has been no systematic analysis of modeling work combined with ROV observation data to simulate methane processes in cold seeps and mud volcano regions. Considering that diffusion-dominated methane processes in sediments are extremely slow and insignificantly impact on human life (Jørgensen and Kasten, 2006; Regnier et al., 2011), it would be more meaningful to simulate large-scale methane leakage in cold seeps and mud volcano regions. Better modeling work on methane dynamics in extreme environments and under changing environmental conditions can help improve the methane cycle predictive capability.

AUTHOR CONTRIBUTIONS

ZS and SX jointly put forward the research objectives of this task, formulated the research route, wrote and organized this research together with ZW, WG, and HC: Data curation, Formal analysis. XZ and BZ: Review and editing.

FUNDING

This study was supported by the Natural Science Foundation of China (42176057, 41376077, and 41976057), the Shandong Special Fund of Pilot National Laboratory for Marine Science and Technology (Qingdao) (2021QNLM020002), and the Marine Geological Survey Program of China Geological Survey (DD20221707).

REFERENCES

Adler, M., Hensen, C., Kasten, S., and Schulz, H. D. (2000). Computer Simulation of Deep Sulfate Reduction in Sediments of the Amazon Fan. *Int. J. earth Sci.* 88 (4), 641–654. doi:10.1007/s005310050294

Akam, S. A., Coffin, R. B., Abdulla, H. A. N., and Lyons, T. W. (2020). Dissolved Inorganic Carbon Pump in Methane-Charged Shallow Marine Sediments: State of the Art and New Model Perspectives. *Front. Mar. Sci.* 7, 206. doi:10.3389/fmars.2020.00206

Albert, D. B., Martens, C. S., and Alperin, M. J. (1998). Biogeochemical Processes Controlling Methane in Gassy Coastal Sediments—Part 2: Groundwater Flow Control of Acoustic Turbidity in Eckernförde Bay Sediments. *Continental Shelf Res.* 18 (14-15), 1771–1793. doi:10.1016/S0278-4343(98)00057-0

Allen, M. R., Shine, K. P., Fuglestvedt, J. S., Millar, R. J., Cain, M., Frame, D. J., et al. (2018). A Solution to the Misrepresentations of CO_2-equivalent Emissions of Short-Lived Climate Pollutants Under Ambitious Mitigation. *Npj Clim. Atmos. Sci.* 1 (1), 1–8. doi:10.1038/s41612-018-0026-8

Aloisi, G., Wallmann, K., Haese, R. R., and Saliège, J.-F. (2004). Chemical, Biological and Hydrological Controls on the ^{14}C Content of Cold Seep Carbonate Crusts: Numerical Modeling and Implications for Convection at Cold Seeps. *Chem. Geology.* 213 (4), 359–383. doi:10.1016/j.chemgeo.2004.07.008

Anderson, A., Abegg, F., Hawkins, J., Duncan, M., and Lyons, A. (1998). Bubble Populations and Acoustic Interaction with the Gassy Floor of Eckernförde Bay. *Continental Shelf Res.* 18 (14-15), 1807–1838. doi:10.1016/S0278-4343(98)00059-4

Anderson, T. R., Hawkins, E., and Jones, P. D. (2016). CO_2, the Greenhouse Effect and Global Warming: from the Pioneering Work of Arrhenius and Callendar to Today's Earth System Models. *Endeavour.* 40 (3), 178–187. doi:10.1016/j.endeavour.2016.07.002

Andreassen, K., Hogstad, K., and Berteussen, K. A. (1990). Gas Hydrate in the Southern Barents Sea, Indicated by a Shallow Seismic Anomaly. *First Break* 8, 235–245. doi:10.3997/1365-2397.1990012

Andreassen, K., Hubbard, A., Winsborrow, M., Patton, H., Vadakkepuliyambatta, S., Plaza-Faverola, A., et al. (2017). Massive Blow-Out Craters Formed by Hydrate-Controlled Methane Expulsion from the Arctic Seafloor. *Science* 356, 948–953. doi:10.1126/science.aal4500

Archer, D., Buffett, B., and Brovkin, V. (2009). Ocean Methane Hydrates as a Slow Tipping point in the Global Carbon Cycle. *Proc. Natl. Acad. Sci. U.S.A.* 106 (49), 20596–20601. doi:10.1073/pnas.0800885105

Archer, D. E., Morford, J. L., and Emerson, S. R. (2002). A Model of Suboxic Sedimentary Diagenesis Suitable for Automatic Tuning and Gridded Global Domains. *Glob. Biogeochem. Cycles* 16 (1), 17–11721. doi:10.1029/2000GB001288

Arndt, S., Brumsack, H.-J., and Wirtz, K. W. (2006). Cretaceous Black Shales as Active Bioreactors: a Biogeochemical Model for the Deep Biosphere Encountered during ODP Leg 207 (Demerara Rise). *Geochimica et Cosmochimica Acta.* 70 (2), 408–425. doi:10.1016/j.gca.2005.09.010

Arndt, S., Hetzel, A., and Brumsack, H.-J. (2009). Evolution of Organic Matter Degradation in Cretaceous Black Shales Inferred from Authigenic Barite: A

Reaction-Transport Model. *Geochimica et Cosmochimica Acta.* 73 (7), 2000–2022. doi:10.1016/j.gca.2009.01.018

Arndt, S., Jørgensen, B. B., LaRowe, D. E., Middelburg, J. J., Pancost, R. D., and Regnier, P. (2013). Quantifying the Degradation of Organic Matter in marine Sediments: a Review and Synthesis. *Earth-science Rev.* 123, 53–86. doi:10.1016/j.earscirev.2013.02.008

Artemov, Y. G., Egorov, V., Polikarpov, G., and Gulin, S. (2007). Methane Emission to the Hydro-And Atmosphere by Gas Bubble Streams in the Dnieper Paleo-Delta, the Black Sea. *Mar. Ecol. J.* 6 (3), 5–26.

Barnes, R. O., and Goldberg, E. D. (1976). Methane Production and Consumption in Anoxic marine Sediments. *Geology* 4 (5), 297–300. doi:10.1130/0091-7613(1976)4<297:mpacia>2.0.co;2

Bastviken, D., Cole, J., Pace, M., and Tranvik, L. (2004). Methane Emissions From Lakes: Dependence of Lake Characteristics, Two Regional Assessments, and a Global Estimate. *Glob. Biogeochem. Cycles* 18 (4), a–n. doi:10.1029/2004GB002238

Beal, E. J., House, C. H., and Orphan, V. J. (2009). Manganese- and Iron-Dependent Marine Methane Oxidation. *Science* 325, 184–187. doi:10.1126/science.1169984

Ben-Avraham, Z., Smith, G., Reshef, M., and Jungslager, E. (2002). Gas Hydrate and Mud Volcanoes on the Southwest African Continental Margin off South Africa. *Geology* 30 (10), 927–930. doi:10.1130/0091-7613(2002)030<0927:ghamvo>2.0.co;2

Berner, R. A. (2020). *Early Diagenesis: A Theoretical Approach*. Princeton, NJ: Princeton University Press.

Blair, N. E., and Aller, R. C. (1995). Anaerobic Methane Oxidation on the Amazon Shelf. *Geochimica et Cosmochimica Acta.* 59 (18), 3707–3715. doi:10.1016/0016-7037(95)00277-7

Blair, N. (1998). The $\delta^{13}C$ of Biogenic Methane in marine Sediments: the Influence of Corg Deposition Rate. *Chem. Geology.* 152 (1-2), 139–150. doi:10.1016/S0009-2541(98)00102-8

Blomberg, A. E. A., Saebo, T. O., Hansen, R. E., Pedersen, R. B., and Austeng, A. (2017). Automatic Detection of marine Gas Seeps Using an Interferometric Sidescan Sonar. *IEEE J. Oceanic Eng.* 42 (3), 590–602. doi:10.1109/JOE.2016.2592559

Boetius, A., and Wenzhöfer, F. (2013). Seafloor Oxygen Consumption Fuelled by Methane From Cold Seeps. *Nat. Geosci.* 6 (9), 725–734. doi:10.1038/ngeo1926

Bohrmann, G., Greinert, J., Suess, E., and Torres, M. (1998). Authigenic Carbonates from the Cascadia Subduction Zone and Their Relation to Gas Hydrate Stability. *Geology* 26 (7), 6472–6650. doi:10.1130/0091-7613(1998)026<0647:acftcs>2.3.co;2

Boles, J. R., Clark, J. F., Leifer, I., and Washburn, L. (2001). Temporal Variation in Natural Methane Seep Rate Due to Tides, Coal Oil Point Area, California. *J. Geophys. Res.* 106 (C11), 27077–27086. doi:10.1029/2000JC000774

Borges, A. V., Champenois, W., Gypens, N., Delille, B., and Harlay, J. (2016). Massive marine Methane Emissions from Near-Shore Shallow Coastal Areas. *Sci. Rep.* 6 (1), 1–8. doi:10.1038/srep27908

Borowski, W. S., Hoehler, T. M., Alperin, M. J., Rodriguez, N. M., and Paull, C. K. (2000). Significance of Anaerobic Methane Oxidation in Methane-Rich Sediments Overlying the Blake Ridge Gas Hydrates. *Dillon, Proceedings ODP, Scientific Results*. Editors C. K. Paull, R. Matsumoto, P. J. Wallace, and W. P. Dillon (College Station, TX: Ocean Drilling Program) 164, 87–99.

Boswell, R. (2009). Gulf of Mexico Gas Hydrate Drilling and Logging Expedition Underway. *Nat. Gas Oil.* 304, 285–4541.

Boudreau, B. P. (1996). A Method-Of-Lines Code for Carbon and Nutrient Diagenesis in Aquatic Sediments. *Comput. Geosciences.* 22 (5), 479–496. doi:10.1016/0098-3004(95)00115-8

Boudreau, B. P. (1997). *Diagenetic Models and Their Implementation*. Berlin: Springer.

Boudreau, B. P., Mucci, A., Sundby, B., Luther, G. W., and Silverberg, N. (1998). Comparative Diagenesis at Three Sites on the Canadian continental Margin. *J. Mar. Res.* 56 (6), 1259–1284. doi:10.1357/002224098765093634

Boudreau, B. P., and Ruddick, B. R. (1991). On a Reactive Continuum Representation of Organic Matter Diagenesis. *Am. J. Sci.* 291 (5), 507–538. doi:10.2475/ajs.291.5.507

Bousquet, P., Ciais, P., Miller, J. B., Dlugokencky, E. J., Hauglustaine, D. A., Prigent, C., et al. (2006). Contribution of Anthropogenic and Natural Sources to Atmospheric Methane Variability. *Nature* 443 (7110), 439–443. doi:10.1038/nature05132

Bovensmann, H., Buchwitz, M., Burrows, J. P., Reuter, M., Krings, T., Gerilowski, K., et al. (2010). A Remote Sensing Technique for Global Monitoring of Power Plant CO_2 Emissions From Space and Related Applications. *Atmos. Meas. Tech.* 3 (4), 781–811. doi:10.5194/amt-3-781-2010

Briggs, G. (1969). Optimum Formulas for Buoyant Plume Rise. *Philosophical Trans. R. Soc. Lond. Ser. A, Math. Phys. Sci.* 265 (1161), 197–203.

Brooks, J. M., Anderson, A. L., Sassen, R., Kennicutt, M. C., and Guinasso, N. L., JR (1994). Hydrate Occurrences in Shallow Subsurface Cores from continental Slope Sediments. *Ann. New York Acad. Sci.* 715 (1), 381–391. doi:10.1111/j.1749-6632.1994.tb38851.x

Buffett, B., and Archer, D. (2004). Global Inventory of Methane Clathrate: Sensitivity to Changes in the Deep Ocean. *Earth Planet. Sci. Lett.* 227 (3-4), 185–199. doi:10.1016/j.epsl.2004.09.005

Burdige, D. J., Komada, T., Magen, C., and Chanton, J. P. (2016). Methane Dynamics in Santa Barbara Basin (USA) Sediments as Examined With a Reaction-Transport Model. *J Mar. Res.* 74 (6), 277–313. doi:10.1357/002224016821744151

Burdige, D. J., and Komada, T. (2015). "Sediment Pore Waters," in *Biogeochemistry of marine Dissolved Organic Matter* (Elsevier), 535–577. doi:10.1016/b978-0-12-405940-5.00012-1

Burwicz, E. B., Rüpke, L. H., and Wallmann, K. (2011). Estimation of the Global Amount of Submarine Gas Hydrates Formed via Microbial Methane Formation Based on Numerical Reaction-Transport Modeling and a Novel Parameterization of Holocene Sedimentation. *Geochimica et Cosmochimica Acta.* 75 (16), 4562–4576. doi:10.1016/j.gca.2011.05.029

Bussmann, I., and Suess, E. (1998). Groundwater Seepage in Eckernförde Bay (Western Baltic Sea): Effect on Methane and Salinity Distribution of the Water Column. *Continental shelf Res.* 18 (14-15), 1795–1806. doi:10.1016/S0278-4343(98)00058-2

Canfield, D. E., Thamdrup, B., and Hansen, J. W. (1993). The Anaerobic Degradation of Organic Matter in Danish Coastal Sediments: Iron Reduction, Manganese Reduction, and Sulfate Reduction. *Geochimica et Cosmochimica Acta.* 57 (16), 3867–3883. doi:10.1016/0016-7037(93)90340-3

Caprais, J.-C., Lanteri, N., Crassous, P., Noel, P., Bignon, L., Rousseaux, P., et al. (2010). A New CALMAR Benthic Chamber Operating by Submersible: First Application in the Cold-Seep Environment of Napoli Mud Volcano (Mediterranean Sea). *Limnol. Oceanogr. Methods.* 8 (6), 304–312. doi:10.4319/lom.2010.8.304

Chanton, J. P., Martens, C. S., and Kelley, C. A. (1989). Gas Transport From Methane-Saturated, Tidal Freshwater and Wetland Sediments. *Limnol. Oceanogr.* 34 (5), 807–819. doi:10.4319/lo.1989.34.5.0807

Chen, N. C., Yang, T. F., Hong, W. L., Chen, H. W., Chen, H. C., Hu, C. Y., et al. (2017). Production, Consumption, and Migration of Methane in Accretionary Prism of Southwestern Taiwan. *Geochem. Geophys. Geosyst.* 18, 2970–2989. doi:10.1002/2017GC006798

Chuang, P.-C., Yang, T. F., Wallmann, K., Matsumoto, R., Hu, C.-Y., Chen, H.-W., et al. (2019). Carbon Isotope Exchange during Anaerobic Oxidation of Methane (AOM) in Sediments of the Northeastern South China Sea. *Geochimica et Cosmochimica Acta.* 246, 138–155. doi:10.1016/j.gca.2018.11.003

Clift, R., Grace, J. R., and Weber, M. E. (2005). *Bubbles, Drops, and Particles*. Courier Corporation.

Conrad, R. (2005). Quantification of Methanogenic Pathways Using Stable Carbon Isotopic Signatures: a Review and a Proposal. *Org. Geochem.* 36 (5), 739–752. doi:10.1016/j.orggeochem.2004.09.006

Crespo-Medina, M., Meile, C. D., Hunter, K. S., Diercks, A.-R., Asper, V. L., Orphan, V. J., et al. (2014). The Rise and Fall of Methanotrophy Following a Deepwater Oil-Well Blowout. *Nat. Geosci.* 7 (6), 423–427. doi:10.1038/ngeo2156

Crill, P. M., and Martens, C. S. (1987). Biogeochemical Cycling in an Organic-Rich Coastal marine basin. 6. Temporal and Spatial Variations in Sulfate Reduction Rates. *Geochimica et Cosmochimica Acta.* 51 (5), 1175–1186. doi:10.1016/0016-7037(87)90210-9

Dale, A. W., Aguilera, D. R., Regnier, P., Fossing, H., Knab, N. J., and Jørgensen, B. B. (2008a). Seasonal Dynamics of the Depth and Rate of Anaerobic Oxidation of Methane in Aarhus Bay (Denmark) Sediments. *J. Mar. Res.* 66 (1), 127–155. doi:10.1357/002224008784815775

Dale, A. W., Regnier, P., Knab, N. J., Jørgensen, B. B., and Van Cappellen, P. (2008b). Anaerobic Oxidation of Methane (AOM) in marine Sediments from the Skagerrak (Denmark): II. Reaction-Transport Modeling. *Geochimica et Cosmochimica Acta* 72 (12), 2880–2894. doi:10.1016/j.gca.2007.11.039

Dale, A. W., Van Cappellen, P., Aguilera, D. R., and Regnier, P. (2008c). Methane Efflux From Marine Sediments in Passive and Active Margins: Estimations From Bioenergetic Reaction–Transport Simulations. *Earth Planet. Sci. Lett.* 265 (3-4), 329–344. doi:10.1016/j.epsl.2007.09.026

Dale, A. W., Brüchert, V., Alperin, M., and Regnier, P. (2009). An Integrated Sulfur Isotope Model for Namibian Shelf Sediments. *Geochimica et Cosmochimica Acta.* 73 (7), 1924–1944. doi:10.1016/j.gca.2008.12.015

Dale, A. W., Flury, S., Fossing, H., Regnier, P., Røy, H., Scholze, C., et al. (2019). Kinetics of Organic Carbon Mineralization and Methane Formation in marine Sediments (Aarhus Bay, Denmark). *Geochimica et Cosmochimica Acta.* 252, 159–178. doi:10.1016/j.gca.2019.02.033

Dale, A. W., Regnier, P., and Van Cappellen, P. (2006). Bioenergetic Controls on Anaerobic Oxidation of Methane (AOM) in Coastal Marine Sediments: a Theoretical Analysis. *Am. J. Sci.* 306 (4), 246–294. doi:10.2475/ajs.306.4.246

Dale, A. W., Sommer, S., Haeckel, M., Wallmann, K., Linke, P., Wegener, G., et al. (2010). Pathways and Regulation of Carbon, Sulfur and Energy Transfer in marine Sediments Overlying Methane Gas Hydrates on the Opouawe Bank (New Zealand). *Geochimica et Cosmochimica Acta.* 74 (20), 5763–5784. doi:10.1016/j.gca.2010.06.038

Davidson, D. W., Garg, S. K., Gough, S. R., Handa, Y. P., Ratcliffe, C. I., Ripmeester, J. A., et al. (1986). Laboratory Analysis of a Naturally Occurring Gas Hydrate from Sediment of the Gulf of Mexico. *Geochimica et Cosmochimica Acta.* 50 (4), 619–623. doi:10.1016/0016-7037(86)90110-9

Davie, M. K., and Buffett, B. A. (2001). A Numerical Model for the Formation of Gas Hydrate below the Seafloor. *J. Geophys. Res.* 106 (B1), 497–514. doi:10.1029/2000JB900363

Decker, C., Caprais, J.-C., Khripounoff, A., and Olu, K. (2012). First Respiration Estimates of Cold-Seep Vesicomyid Bivalves From *In Situ* Total Oxygen Uptake Measurements. *Comptes rendus biologies.* 335 (4), 261–270. doi:10.1016/j.crvi.2012.03.002

Devol, A. H., Anderson, J. J., Kuivila, K., and Murray, J. W. (1984). A Model for Coupled Sulfate Reduction and Methane Oxidation in the Sediments of Saanich Inlet. *Geochimica et cosmochimica acta.* 48 (5), 993–1004. doi:10.1016/0016-7037(84)90191-1

Dickens, G. R., Castillo, M. M., and Walker, J. C. G. (1997). A Blast of Gas in the Latest Paleocene: Simulating First-Order Effects of Massive Dissociation of Oceanic Methane Hydrate. *Geology.* 25 (3), 259–262. doi:10.1130/0091-7613(1997)025<0259:abogit>2.3.co;2

Dickens, G. R., and Quinby-Hunt, M. S. (1994). Methane Hydrate Stability in Seawater. *Geophys. Res. Lett.* 21 (19), 2115–2118. doi:10.1029/94GL01858

Dickens, G. R. (2001). The Potential Volume of Oceanic Methane Hydrates With Variable External Conditions. *Org. Geochem.* 32 (10), 1179–1193. doi:10.1016/S0146-6380(01)00086-9

Dlugokencky, E. J., Nisbet, E. G., Fisher, R., and Lowry, D. (2011). Global Atmospheric Methane: Budget, Changes and Dangers. *Phil. Trans. R. Soc. A.* 369 (1943), 2058–2072. doi:10.1098/rsta.2010.0341

Duan, Z., and Weare, J. H. (1992). Reply to Comment by J. J. Carroll on "The Prediction of Methane Solubility in Natural Waters to High Ionic Strength from 0 to 250°C and from 0 to 1600 Bar". *Geochimica et Cosmochimica Acta* 56, 4303. doi:10.1016/0016-7037(92)90215-510.1016/0016-7037(92)90271-j

Dunne, J. P., Sarmiento, J. L., and Gnanadesikan, A. (2007). A Synthesis of Global Particle Export From the Surface Ocean and Cycling Through the Ocean Interior and on the Seafloor. *Glob. Biogeochem. Cycles.* 21 (4), a–n. doi:10.1029/2006GB002907

Egger, M., Rasigraf, O., Sapart, C. J., Jilbert, T., Jetten, M. S. M., Röckmann, T., et al. (2015). Iron-Mediated Anaerobic Oxidation of Methane in Brackish Coastal Sediments. *Environ. Sci. Technol.* 49 (1), 277–283. doi:10.1021/es503663z

Egger, M., Riedinger, N., Mogollón, J. M., and Jørgensen, B. B. (2018). Global Diffusive Fluxes of Methane in marine Sediments. *Nat. Geosci.* 11 (6), 421–425. doi:10.1038/s41561-018-0122-8

Etminan, M., Myhre, G., Highwood, E. J., and Shine, K. P. (2016). Radiative Forcing of Carbon Dioxide, Methane, and Nitrous Oxide: A Significant Revision of the Methane Radiative Forcing. *Geophys. Res. Lett.* 43 (2412), 614623–615612. doi:10.1002/2016GL071930

Ettwig, K. F., Zhu, B., Speth, D., Keltjens, J. T., Jetten, M. S. M., and Kartal, B. (2016). Archaea Catalyze Iron-Dependent Anaerobic Oxidation of Methane. *Proc. Natl. Acad. Sci. U.S.A.* 113 (45), 12792–12796. doi:10.1073/pnas.1609534113

Felden, J., Lichtschlag, A., Wenzhöfer, F., de Beer, D., Feseker, T., Pop Ristova, P., et al. (2013). Limitations of Microbial Hydrocarbon Degradation at the Amon Mud Volcano (Nile Deep-Sea Fan). *Biogeosciences.* 10 (5), 3269–3283. doi:10.5194/bg-10-3269-2013

Fenchel, T., Blackburn, H., King, G. M., and Blackburn, T. H. (2012). *Bacterial Biogeochemistry: The Ecophysiology of mineral Cycling*. Cambridge, MA: Academic Press.

Ferré, B., Jansson, P. G., Moser, M., Serov, P., Portnov, A., Graves, C. A., et al. (2020). Reduced Methane Seepage From Arctic Sediments During Cold Bottom-Water Conditions. *Nat. Geosci.* 13 (2), 144–148. doi:10.1038/s41561-019-0515-3

Fischer, D., Mogollón, J. M., Strasser, M., Pape, T., Bohrmann, G., Fekete, N., et al. (2013). Subduction Zone Earthquake as Potential Trigger of Submarine Hydrocarbon Seepage. *Nat. Geosci.* 6 (8), 647–651. doi:10.1038/ngeo1886

Fossing, H., Ferdelman, T. G., and Berg, P. (2000). Sulfate Reduction and Methane Oxidation in Continental Margin Sediments Influenced by Irrigation (South-East Atlantic off Namibia). *Geochimica et Cosmochimica Acta.* 64 (5), 897–910. doi:10.1016/S0016-7037(99)00349-X

Freire, A. F. M., Matsumoto, R., and Santos, L. A. (2011). Structural-stratigraphic Control on the Umitaka Spur Gas Hydrates of Joetsu Basin in the Eastern Margin of Japan Sea. *Mar. Pet. Geology.* 28, 1967–1978. doi:10.1016/j.marpetgeo.2010.10.004

Fu, X., Waite, W. F., and Ruppel, C. D. (2021). Hydrate Formation on Marine Seep Bubbles and the Implications for Water Column Methane Dissolution. *J. Geophys. Res. Oceans.* 126 (9), e2021JC017363. doi:10.1029/2021JC017363

Gentz, T., Damm, E., Schneider von Deimling, J., Mau, S., McGinnis, D. F., and Schlüter, M. (2014). A Water Column Study of Methane Around Gas Flares Located at the West Spitsbergen continental Margin. *Continental Shelf Res.* 72, 107–118. doi:10.1016/j.csr.2013.07.013

Gerilowski, K., Krings, T., Hartmann, J., Buchwitz, M., Sachs, T., Erzinger, J., et al. (2015). Atmospheric Remote Sensing Constraints on Direct Sea-Air Methane Flux from the 22/4b North Sea Massive Blowout Bubble Plume. *Mar. Pet. Geology.* 68, 824–835. doi:10.1016/j.marpetgeo.2015.07.011

Giustiniani, M., Tinivella, U., Sauli, C., and Della Vedova, B. (2018). Distribution of the Gas Hydrate Stability Zone in the Ross Sea, Antarctica. *Andean Geology.* 45 (1), 78–86. doi:10.5027/andgeoV45n1-2989

Graves, C. A., Steinle, L., Rehder, G., Niemann, H., Connelly, D. P., Lowry, D., et al. (2015). Fluxes and Fate of Dissolved Methane Released at the Seafloor at the Landward Limit of the Gas Hydrate Stability Zone Offshore Western Svalbard. *J. Geophys. Res. Oceans.* 120, 6185–6201. doi:10.1002/2015JC011084

Grünke, S., Felden, J., Lichtschlag, A., Girnth, A.-C., de Beer, D., Wenzhöfer, F., et al. (2011). Niche Differentiation Among Mat-Forming, Sulfide-Oxidizing Bacteria at Cold Seeps of the Nile Deep Sea Fan (Eastern Mediterranean Sea). *Geobiology* 9 (4), 330–348. doi:10.1111/j.1472-4669.2011.00281.x

Haeckel, M. (2006). "A Transport-Reaction Model of the Hydrological Systems of the Costa Rica Subduction Zone," in Proceedings of the Ocean Drilling Program, Scientific Results, Leg), 1–26.

Haeckel, M., Boudreau, B. P., and Wallmann, K. (2007). Bubble-Induced Porewater Mixing: A 3-D Model for Deep Porewater Irrigation. *Geochimica et Cosmochimica Acta.* 71 (21), 5135–5154. doi:10.1016/j.gca.2007.08.011

Haese, R. R., Meile, C., Van Cappellen, P., and De Lange, G. J. (2003). Carbon Geochemistry of Cold Seeps: Methane Fluxes and Transformation in Sediments from Kazan Mud Volcano, Eastern Mediterranean Sea. *Earth Planet. Sci. Lett.* 212, 361–375. doi:10.1016/S0012-821X(03)00226-7

Hensen, C., and Wallmann, K. (2005). Methane Formation at Costa Rica Continental Margin-Constraints for Gas Hydrate Inventories and Cross-Décollement Fluid Flow. *Earth Planet. Sci. Lett.* 236 (1-2), 41–60. doi:10.1016/j.epsl.2005.06.007

Higgs, B., Mountjoy, J. J., Crutchley, G. J., Townend, J., Ladroit, Y., Greinert, J., et al. (2019). Seep-bubble Characteristics and Gas Flow Rates from a Shallow-Water, High-Density Seep Field on the Shelf-To-Slope Transition of the Hikurangi Subduction Margin. *Mar. Geology.* 417, 105985. doi:10.1016/j.margeo.2019.105985

Hiruta, A., Snyder, G. T., Tomaru, H., and Matsumoto, R. (2009). Geochemical Constraints for the Formation and Dissociation of Gas Hydrate in an Area of High Methane Flux, Eastern Margin of the Japan Sea. *Earth Planet. Sci. Lett.* 279 (3-4), 326–339. doi:10.1016/j.epsl.2009.01.015

Holmes, M. E., Sansone, F. J., Rust, T. M., and Popp, B. N. (2000). Methane Production, Consumption, and Air-Sea Exchange in the Open Ocean: An Evaluation Based on Carbon Isotopic Ratios. *Glob. Biogeochem. Cycles.* 14 (1), 1–10. doi:10.1029/1999GB001209

Hovland, M., Judd, A. G., and Burke, R., Jr (1993). The Global Flux of Methane from Shallow Submarine Sediments. *Chemosphere.* 26 (1-4), 559–578. doi:10.1016/0045-6535(93)90442-8

Inagaki, F., Nunoura, T., Nakagawa, S., Teske, A., Lever, M., Lauer, A., et al. (2006). Biogeographical Distribution and Diversity of Microbes in Methane Hydrate-Bearing Deep Marine Sediments on the Pacific Ocean Margin. *Proc. Natl. Acad. Sci. U.S.A.* 103 (8), 2815–2820. doi:10.1073/pnas.0511033103

Jørgensen, B. B. (1978). A Comparison of Methods for the Quantification of Bacterial Sulfate Reduction in Coastal marine Sediments. *Geomicrobiology J.* 1 (1), 11–27. doi:10.1080/01490457809377721

Jahren, A. H., Arens, N. C., Sarmiento, G., Guerrero, J., and Amundson, R. (2001). Terrestrial Record of Methane Hydrate Dissociation in the Early Cretaceous. *Geology* 29 (2), 159–162. doi:10.1130/0091-7613(2001)029<0159:tromhd>2.0.co;2

Jakosky, B. M., Henderson, B. G., and Mellon, M. T. (1995). Chaotic Obliquity and the Nature of the Martian Climate. *J. Geophys. Res.* 100 (E1), 1579–1584. doi:10.1029/94JE02801

Jiang, H., and Breier, J. A. (2014). Physical Controls on Mixing and Transport within Rising Submarine Hydrothermal Plumes: A Numerical Simulation Study. *Deep Sea Res. Oceanographic Res. Pap.* 92, 41–55. doi:10.1016/j.dsr.2014.06.006

Johansen, C., Macelloni, L., Natter, M., Silva, M., Woosley, M., Woolsey, A., et al. (2020). Hydrocarbon Migration Pathway and Methane Budget for a Gulf of Mexico Natural Seep Site: Green Canyon 600. *Earth Planet. Sci. Lett.* 545, 116411. doi:10.1016/j.epsl.2020.116411

Jørgensen, B. B., Böttcher, M. E., Lüschen, H., Neretin, L. N., and Volkov, I. I. (2004). Anaerobic Methane Oxidation and a Deep H2S Sink Generate Isotopically Heavy Sulfides in Black Sea Sediments. *Geochimica et Cosmochimica Acta* 68 (9), 2095–2118. doi:10.1016/j.gca.2003.07.017

Jørgensen, S. E., and Kasten, S. (2006). Sulfur Cycling and Methane Oxidation. *Ecol. Model.* 196, 271–309. doi:10.1016/j.ecolmodel.2006.03.010

Keppler, F., Boros, M., Frankenberg, C., Lelieveld, J., McLeod, A., Pirttilä, A. M., et al. (2009). Methane Formation in Aerobic Environments. *Environ. Chem.* 6 (6), 459–465. doi:10.1071/EN09137

Klauda, J. B., and Sandler, S. I. (2005). Global Distribution of Methane Hydrate in Ocean Sediment. *Energy Fuels.* 19, 459–470. doi:10.1021/ef049798o

Knab, N. J., Cragg, B. A., Borowski, C., Parkes, R. J., Pancost, R., and Jørgensen, B. B. (2008). Anaerobic Oxidation of Methane (AOM) in marine Sediments from the Skagerrak (Denmark): I. Geochemical and Microbiological Analyses. *Geochimica et Cosmochimica Acta.* 72 (12), 2868–2879. doi:10.1016/j.gca.2008.03.016

Krapivin, V. F., Varotsos, C. A., and Soldatov, V. Y. (2017). Simulation Results from a Coupled Model of Carbon Dioxide and Methane Global Cycles. *Ecol. Model.* 359, 69–79. doi:10.1016/j.ecolmodel.2017.05.023

Kretschmer, K., Biastoch, A., Rüpke, L., and Burwicz, E. (2015). Modeling the Fate of Methane Hydrates under Global Warming. *Glob. Biogeochem. Cycles.* 29 (5), 610–625. doi:10.1002/2014GB005011

Kvenvolden, K. A. (1993). Gas Hydrates-Geological Perspective and Global Change. *Rev. Geophys.* 31 (2), 173–187. doi:10.1029/93RG00268

Kvenvolden, K. A., and Kastner, M. (1990). "32. Gas Hydrates of the Peruvian Outer continental Margin1," in Proceedings of the Ocean Drilling Program, Scientific Results: Citeseer), 517–526.

Larcombe, P., Carter, R., Dye, J., Gagan, M., and Johnson, D. (1995). New Evidence for Episodic post-glacial Sea-Level Rise, central Great Barrier Reef, Australia. *Mar. Geology.* 127 (1-4), 1–44. doi:10.1016/0025-3227(95)00059-8

LaRowe, D. E., Arndt, S., Bradley, J. A., Estes, E. R., Hoarfrost, A., Lang, S. Q., et al. (2020). The Fate of Organic Carbon in marine Sediments - New Insights from Recent Data and Analysis. *Earth-Science Rev.* 204, 103146. doi:10.1016/j.earscirev.2020.103146

Leifer, I., and Judd, A. (2015). The UK22/4b Blowout 20 Years on: Investigations of Continuing Methane Emissions from Sub-seabed to the Atmosphere in a North Sea Context. *Mar. Pet. Geology.* 68, 706–717. doi:10.1016/j.marpetgeo.2015.11.012

Leifer, I., Luyendyk, B. P., Boles, J., and Clark, J. F. (2006). Natural Marine Seepage Blowout: Contribution to Atmospheric Methane. *Glob. Biogeochem. Cycles.* 20, a–n. doi:10.1029/2005GB002668

Leifer, I., and Patro, R. K. (2002). The Bubble Mechanism for Methane Transport from the Shallow Sea Bed to the Surface: A Review and Sensitivity Study. *Continental Shelf Res.* 22 (16), 2409–2428. doi:10.1016/S0278-4343(02)00065-1

Lelieveld, J., Peters, W., Dentener, F. J., and Krol, M. C. (2002). Stability of Tropospheric Hydroxyl Chemistry. *J.-Geophys.-Res.* 107 (D23), 17–21. doi:10.1029/2002JD002272

Lenhart, K., Klintzsch, T., Langer, G., Nehrke, G., Bunge, M., Schnell, S., et al. (2015). Evidence for Methane Production by marine Algae (Emiliana Huxleyi) and its Implication for the Methane Paradox in Oxic Waters. *Biogeosciences Discuss.* 12, 20323–20360. doi:10.5194/bgd-12-20323-201

Li, J.-f., Ye, J.-l., Ye, J.-l., Qin, X.-w., Qiu, H.-j., Wu, N.-y., et al. (2018). The First Offshore Natural Gas Hydrate Production Test in South China Sea. *China Geology.* 1 (1), 5–16. doi:10.31035/cg2018003

Lichtschlag, A., Felden, J., Wenzhöfer, F., Schubotz, F., Ertefai, T. F., Boetius, A., et al. (2010). Methane and Sulfide Fluxes in Permanent Anoxia: *In Situ* Studies at the Dvurechenskii Mud Volcano (Sorokin Trough, Black Sea). *Geochimica et Cosmochimica Acta.* 74 (17), 5002–5018. doi:10.1016/j.gca.2010.05.031

Linke, P., Wallmann, K., Suess, E., Hensen, C., and Rehder, G. (2005). *In Situ* benthic Fluxes from an Intermittently Active Mud Volcano at the Costa Rica Convergent Margin. *Earth Planet. Sci. Lett.* 235, 79–95. doi:10.1016/j.epsl.2005.03.009

Lohrberg, A., Schmale, O., Ostrovsky, I., Niemann, H., Held, P., and Schneider von Deimling, J. (2020). Discovery and Quantification of a Widespread Methane Ebullition Event in a Coastal Inlet (Baltic Sea) Using a Novel Sonar Strategy. *Sci. Rep.* 10 (1), 1–13. doi:10.1038/s41598-020-60283-0

Luff, R., Greinert, J., Wallmann, K., Klaucke, I., and Suess, E. (2005). Simulation of Long-Term Feedbacks from Authigenic Carbonate Crust Formation at Cold Vent Sites. *Chem. Geology.* 216 (1-2), 157–174. doi:10.1016/j.chemgeo.2004.11.002

Luff, R., Wallmann, K., and Aloisi, G. (2004). Numerical Modeling of Carbonate Crust Formation at Cold Vent Sites: Significance for Fluid and Methane Budgets and Chemosynthetic Biological Communities. *Earth Planet. Sci. Lett.* 221, 337–353. doi:10.1016/S0012-821X(04)00107-4

Luff, R., and Wallmann, K. (2003). Fluid Flow, Methane Fluxes, Carbonate Precipitation and Biogeochemical Turnover in Gas Hydrate-Bearing Sediments at Hydrate Ridge, Cascadia Margin: Numerical Modeling and Mass Balances. *Geochimica et Cosmochimica Acta.* 67, 3403–3421. doi:10.1016/S0016-7037(03)00127-3

MacDonald, I. R., Guinasso, N. L., Jr, Sassen, R., Brooks, J. M., Lee, L., and Scott, K. T. (1994). Gas Hydrate that Breaches the Sea Floor on the continental Slope of the Gulf of Mexico. *Geology.* 22 (8), 699–702. doi:10.1130/0091-7613(1994)022<0699:ghtbts>2.3.co;2

Maher, K., Steefel, C. I., DePaolo, D. J., and Viani, B. E. (2006). The Mineral Dissolution Rate Conundrum: Insights from Reactive Transport Modeling of U Isotopes and Pore Fluid Chemistry in marine Sediments. *Geochimica et Cosmochimica Acta.* 70 (2), 337–363. doi:10.1016/j.gca.2005.09.001

Marquardt, M., Hensen, C., Piñero, E., Wallmann, K., and Haeckel, M. (2010). A Transfer Function for the Prediction of Gas Hydrate Inventories in marine Sediments. *Biogeosciences.* 7 (9), 2925–2941. doi:10.5194/bg-7-2925-2010

Martens, C. S., Albert, D. B., and Alperin, M. J. (1998). Biogeochemical Processes Controlling Methane in Gassy Coastal Sediments—Part 1. A Model Coupling Organic Matter Flux to Gas Production, Oxidation and Transport. *Continental Shelf Res.* 18 (14-15), 1741–1770. doi:10.1016/S0278-4343(98)00056-9

Martens, C. S., and Val Klump, J. (1984). Biogeochemical Cycling in an Organic-Rich Coastal Marine basin 4. An Organic Carbon Budget for Sediments Dominated by Sulfate Reduction and Methanogenesis. *Geochimica et Cosmochimica Acta.* 48 (10), 1987–2004. doi:10.1016/0016-7037(84)90380-6

Martens, C. S., and Val Klump, J. (1980). Biogeochemical Cycling in an Organic-Rich Coastal marine basin—I. Methane Sediment-Water Exchange Processes. *Geochimica et Cosmochimica Acta.* 44 (3), 471–490. doi:10.1016/0016-7037(80)90045-9

Mau, S., Tu, T.-H., Becker, M., dos Santos Ferreira, C., Chen, J.-N., Lin, L.-H., et al. (2020). Methane Seeps and Independent Methane Plumes in the South China Sea Offshore Taiwan. *Front. Mar. Sci.* 7, 543. doi:10.3389/fmars.2020.00543

Megonigal, J. P., Hines, M. E., and Visscher, P. T. (2004). Anaerobic Metabolism: Linkages to Trace Gases and Aerobic Processes. *Biogeochemistry*. Editor W. H. Schlesinger (Oxford, UK: Elsevier-Pergamon), 317–424.

Meister, P., Liu, B., Ferdelman, T. G., Jørgensen, B. B., and Khalili, A. (2013). Control of Sulphate and Methane Distributions in Marine Sediments by Organic Matter Reactivity. *Geochimica et Cosmochimica Acta.* 104, 183–193. doi:10.1016/j.gca.2012.11.011

Michel, A. P. M., Preston, V. L., Fauria, K. E., and Nicholson, D. P. (2021). Observations of Shallow Methane Bubble Emissions from Cascadia Margin. *Front. Earth Sci.* 9, 285. doi:10.3389/feart.2021.613234

Middelburg, J. J. (1989). A Simple Rate Model for Organic Matter Decomposition in marine Sediments. *Geochimica et Cosmochimica acta.* 53 (7), 1577–1581. doi:10.1016/0016-7037(89)90239-1

Milkov, A. V. (2004). Global Estimates of Hydrate-Bound Gas in Marine Sediments: How Much Is Really Out There? *Earth-science Rev.* 66 (3-4), 183–197. doi:10.1016/j.earscirev.2003.11.002

Miller, S. L., and Smythe, W. D. (1970). Carbon Dioxide Clathrate in the Martian Ice Cap. *Science* 170 (3957), 531–533. doi:10.1126/science.170.3957.531

Mogollón, J. M., Dale, A. W., L'Heureux, I., and Regnier, P. (2011). Impact of Seasonal Temperature and Pressure Changes on Methane Gas Production, Dissolution, and Transport in Unfractured Sediments. *J. Geophys. Res.* 116 (G3). doi:10.1029/2010JG001592

Mogollón, J. M., L'Heureux, I., Dale, A. W., and Regnier, P. (2009). Methane Gas-phase Dynamics in marine Sediments: A Model Study. *Am. J. Sci.* 309 (3), 189–220. doi:10.2475/03.2009.01

Molins, S., Mayer, K. U., Amos, R. T., and Bekins, B. A. (2010). Vadose Zone Attenuation of Organic Compounds at a Crude Oil Spill Site - Interactions between Biogeochemical Reactions and Multicomponent Gas Transport. *J. Contaminant Hydrol.* 112 (1-4), 15–29. doi:10.1016/j.jconhyd.2009.09.002

Molins, S., and Mayer, K. U. (2007). Coupling Between Geochemical Reactions and Multicomponent Gas and Solute Transport in Unsaturated media: A Reactive Transport Modeling Study. *Water Resour. Res.* 43 (5), n/a. doi:10.1029/2006WR005206

Morton, B., Taylor, G. I., and Turner, J. S. (1956). Turbulent Gravitational Convection from Maintained and Instantaneous Sources. *Proc. R. Soc. Lond. A.* 234 (1196), 1–23. doi:10.1098/rspa.1956.0011

Mrazovac, S. M., Milan, P. R., Vojinovic-Miloradov, M. B., and Tosic, B. S. (2012). Dynamic Model of Methane-Water Diffusion. *Appl. Math. Model.* 36 (9), 3985–3991. doi:10.1016/j.apm.2011.11.009

Muller-Karger, F. E., Varela, R., Thunell, R., Luerssen, R., Hu, C., and Walsh, J. J. (2005). The Importance of continental Margins in the Global Carbon Cycle. *Geophys. Res. Lett.* 32 (1), L01602. doi:10.1029/2004GL021346

Murray, J. W., Grundmanis, V., and Smethie, W. M., Jr (1978). Interstitial Water Chemistry in the Sediments of Saanich Inlet. *Geochimica et Cosmochimica Acta.* 42 (7), 1011–1026. doi:10.1016/0016-7037(78)90290-9

Niemann, H., Lösekann, T., De Beer, D., Elvert, M., Nadalig, T., Knittel, K., et al. (2006). Novel Microbial Communities of the Haakon Mosby Mud Volcano and Their Role as a Methane Sink. *Nature.* 443 (7113), 854–858. doi:10.1038/nature05227

Nisbet, E. G., Manning, M. R., Dlugokencky, E. J., Fisher, R. E., Lowry, D., Michel, S. E., et al. (2019). Very Strong Atmospheric Methane Growth in the 4Years 2014–2017: Implications for the Paris Agreement. *Glob. Biogeochem. Cycles.* 33 (3), 318–342. doi:10.1029/2018GB006009

Nöthen, K., and Kasten, S. (2011). Reconstructing Changes in Seep Activity by Means of Pore Water and Solid Phase Sr/Ca and Mg/Ca Ratios in Pockmark Sediments of the Northern Congo Fan. *Mar. Geology.* 287 (1-4), 1–13. doi:10.1016/j.margeo.2011.06.008

Parkes, R. J., Wellsbury, P., Mather, I. D., Cobb, S. J., Cragg, B. A., Hornibrook, E. R. C., et al. (2007). Temperature Activation of Organic Matter and Minerals during Burial Has the Potential to Sustain the Deep Biosphere over Geological Timescales. *Org. Geochem.* 38 (6), 845–852. doi:10.1016/j.orggeochem.2006.12.011

Paull, C. K., Schlining, B., Ussler, W., III, Paduan, J. B., Caress, D., and Greene, H. G. (2005). Distribution of Chemosynthetic Biological Communities in Monterey Bay, California. *Geology* 33 (2), 85–88. doi:10.1130/G20927.1

Pavlov, A. A., Hurtgen, M. T., Kasting, J. F., and Arthur, M. A. (2003). Methane-Rich Proterozoic Atmosphere? *Geology* 31 (1), 87–90. doi:10.1130/0091-7613(2003)031<0087:mrpa>2.0.co;2

Piñero, E., Marquardt, M., Hensen, C., Haeckel, M., and Wallmann, K. (2013). Estimation of the Global Inventory of Methane Hydrates in marine Sediments Using Transfer Functions. *Biogeosciences* 10 (2), 959–975. doi:10.5194/bg-10-959-2013

Pop Ristova, P., Wenzhöfer, F., Ramette, A., Zabel, M., Fischer, D., Kasten, S., et al. (2012). Bacterial Diversity and Biogeochemistry of Different Chemosynthetic Habitats of the REGAB Cold Seep (West African Margin, 3160 M Water Depth). *Biogeosciences* 9 (12), 5031–5048. doi:10.5194/bg-9-5031-2012

Reagan, M. T., and Moridis, G. J. (2008). Dynamic Response of Oceanic Hydrate Deposits to Ocean Temperature Change. *J. Geophys. Res.* 113 (C12), C12023. doi:10.1029/2008JC004938

Reeburgh, W. S. (1976). Methane Consumption in Cariaco Trench Waters and Sediments. *Earth Planet. Sci. Lett.* 28 (3), 337–344. doi:10.1016/0012-821X(76)90195-3

Reeburgh, W. S. (2007). Oceanic Methane Biogeochemistry. *Chem. Rev.* 107, 486–513. doi:10.1021/cr050362v

Reeburgh, W. S., Ward, B. B., Whalen, S. C., Sandbeck, K. A., Kilpatrickt, K. A., and Kerkhof, L. J. (1991). Black Sea Methane Geochemistry. *Deep Sea Res. A. Oceanographic Res. Pap.* 38, S1189–S1210. doi:10.1016/S0198-0149(10)80030-5

Reed, D. L., Silver, E. A., Tagudin, J. E., Shipley, T. H., and Vrolijk, P. (1990). Relations between Mud Volcanoes, Thrust Deformation, Slope Sedimentation, and Gas Hydrate, Offshore north Panama. *Mar. Pet. Geology.* 7 (1), 44–54. doi:10.1016/0264-8172(90)90055-L

Regnier, P., Dale, A., Pallud, C., Van Lith, Y., Bonneville, S., Hyacinthe, C., et al. (2005). Incorporating Geomicrobial Processes in Subsurface Reactive Transport Models. *Reactive Transport Soil groundwater: Process. models.* Editors G. Nuetzmann, P. Viotti, and P. Agaard (Berlin: Springer-Verlag), 107–126.

Regnier, P., Dale, A. W., Arndt, S., LaRowe, D. E., Mogollón, J., and Van Cappellen, P. (2011). Quantitative Analysis of Anaerobic Oxidation of Methane (AOM) in Marine Sediments: A Modeling Perspective. *Earth-Science Rev.* 106 (1-2), 105–130. doi:10.1016/j.earscirev.2011.01.002

Rehder, G., Leifer, I., Brewer, P. G., Friederich, G., and Peltzer, E. T. (2009). Controls on Methane Bubble Dissolution Inside and outside the Hydrate Stability Field From Open Ocean Field Experiments and Numerical Modeling. *Mar. Chem.* 114 (1-2), 19–30. doi:10.1016/j.marchem.2009.03.004

Repeta, D. J., Ferrón, S., Sosa, O. A., Johnson, C. G., Repeta, L. D., Acker, M., et al. (2016). Marine Methane Paradox Explained by Bacterial Degradation of Dissolved Organic Matter. *Nat. Geosci.* 9 (12), 884–887. doi:10.1038/ngeo2837

Riedel, M., Scherwath, M., Römer, M., Veloso, M., Heesemann, M., and Spence, G. D. (2018). Distributed Natural Gas Venting Offshore along the Cascadia Margin. *Nat. Commun.* 9 (1), 3264–3314. doi:10.1038/s41467-018-05736-x

Römer, M., Hsu, C.-W., Loher, M., MacDonald, I. R., dos Santos Ferreira, C., Pape, T., et al. (2019). Amount and Fate of Gas and Oil Discharged at 3400 M Water Depth from a Natural Seep Site in the Southern Gulf of Mexico. *Front. Mar. Sci.* 6, 700. doi:10.3389/fmars.2019.00700

Römer, M., Sahling, H., dos Santos Ferreira, C., and Bohrmann, G. (2020). Methane Gas Emissions of the Black Sea-Mapping from the Crimean continental Margin to the Kerch Peninsula Slope. *Geo-mar Lett.* 40 (4), 467–480. doi:10.1007/s00367-019-00611-0

Römer, M., Sahling, H., Pape, T., Bahr, A., Feseker, T., Wintersteller, P., et al. (2012). Geological Control and Magnitude of Methane Ebullition from a High-Flux Seep Area in the Black Sea-The Kerch Seep Area. *Mar. Geology.* 319-322, 57–74. doi:10.1016/j.margeo.2012.07.005

Römer, M., Sahling, H., Pape, T., dos Santos Ferreira, C., Wenzhöfer, F., Boetius, A., et al. (2014). Methane Fluxes and Carbonate Deposits at a Cold Seep Area of the Central Nile Deep Sea Fan, Eastern Mediterranean Sea. *Mar. Geology.* 347, 27–42. doi:10.1016/j.margeo.2013.10.011

Römer, M., Wenau, S., Mau, S., Veloso, M., Greinert, J., Schlüter, M., et al. (2017). Assessing marine Gas Emission Activity and Contribution to the Atmospheric Methane Inventory: A Multidisciplinary Approach from the Dutch Dogger

Bank Seep Area (North Sea). *Geochem. Geophys. Geosyst.* 18 (7), 2617–2633. doi:10.1002/2017GC006995

Ruppel, C. D., and Kessler, J. D. (2017). The Interaction of Climate Change and Methane Hydrates. *Rev. Geophys.* 55 (1), 126–168. doi:10.1002/2016RG000534

Sahling, H., Bohrmann, G., Spiess, V., Bialas, J., Breitzke, M., Ivanov, M., et al. (2008). Pockmarks in the Northern Congo Fan Area, SW Africa: Complex Seafloor Features Shaped by Fluid Flow. *Mar. Geology.* 249 (3-4), 206–225. doi:10.1016/j.margeo.2007.11.010

Saito, H., and Suzuki, N. (2007). Terrestrial Organic Matter Controlling Gas Hydrate Formation in the Nankai Trough Accretionary Prism, Offshore Shikoku, Japan. *J. Geochemical Exploration.* 95 (1-3), 88–100. doi:10.1016/j.gexplo.2007.05.007

Sakai, H., Gamo, T., Kim, E.-S., Tsutsumi, M., Tanaka, T., Ishibashi, J., et al. (1990). Venting of Carbon Dioxide-Rich Fluid and Hydrate Formation in Mid-Okinawa Trough Backarc Basin. *Science* 248 (4959), 1093–1096. doi:10.1126/science.248.4959.1093

Saunois, M., Bousquet, P., Poulter, B., Peregon, A., Ciais, P., Canadell, J. G., et al. (2016a). The Global Methane Budget 2000–2012. *Earth Syst. Sci. Data.* 8 (2), 697–751. doi:10.5194/essd-8-697-2016

Saunois, M., Jackson, R. B., Bousquet, P., Poulter, B., and Canadell, J. G. (2016b). The Growing Role of Methane in Anthropogenic Climate Change. *Environ. Res. Lett.* 11, 120207. doi:10.1088/1748-9326/11/12/120207

Schmaljohann, R. (1996). Methane Dynamics in the Sediment and Water Column of Kiel Harbour (Baltic Sea). *Mar. Ecol. Prog. Ser.* 131, 263–273. doi:10.3354/meps131263

Schmidt, M., Hensen, C., Mörz, T., Müller, C., Grevemeyer, I., Wallmann, K., et al. (2005). Methane Hydrate Accumulation in "Mound 11" Mud Volcano, Costa Rica Forearc. *Mar. Geology.* 216 (1-2), 83–100. doi:10.1016/j.margeo.2005.01.001

Scholl, D., and Hart, P. (1993). Velocity and Amplitude Structures on Seismic-Reflection Profiles-Possibly Massive Gas-Hydrate Deposits and Underlying Gas Accumulations in the Bering Sea Basin. *The future of energy gases: U. S. Geological Survey Professional Paper*. Editors D. G. Howell 1570, 331–352.

Schulz, H. D., and Zabel, M. (2006). *Marine Geochemistry*. Berlin: Springer.

Schowalter, T. T. (1979). Mechanics of Secondary Hydrocarbon Migration and Entrapment. *Bulletin.* 63 (5), 723–760. doi:10.1306/2F9182CA-16CE-11D7-8645000102C1865D

Seelig, H. D., Hoehn, A., Stodieck, L. S., Klaus, D. M., Adams, W. W., Iii, and Emery, W. J. (2008). The Assessment of Leaf Water Content Using Leaf Reflectance Ratios in the Visible, Near-, and Short-wave-infrared. *Int. J. Remote Sensing* 29 (13), 3701–3713. doi:10.1080/01431160701772500

Seiter, K., Hensen, C., Schröter, J., and Zabel, M. (2004). Organic Carbon Content in Surface Sediments-Defining Regional Provinces. *Deep Sea Res. Part Oceanographic Res. Pap.* 51 (12), 2001–2026. doi:10.1016/j.dsr.2004.06.014

Shagapov, V. S., Chiglintseva, A. S., Rusinov, A. A., and Tazetdinov, B. I. (2017). Migration of a Single Gas Bubble in Water during the Formation of Stable Gas-Hydrate Crust on its Surface. *Theor. Found. Chem. Eng.* 51 (2), 216–223. doi:10.1134/s0040579517020075

Shakhova, N., Semiletov, I., Leifer, I., Sergienko, V., Salyuk, A., Kosmach, D., et al. (2014). Ebullition and Storm-Induced Methane Release from the East Siberian Arctic Shelf. *Nat. Geosci* 7, 64–70. doi:10.1038/ngeo2007

Shakhova, N., Semiletov, I., Salyuk, A., Yusupov, V., Kosmach, D., and Gustafsson, Ö. (2010). Extensive Methane Venting to the Atmosphere from Sediments of the East Siberian Arctic Shelf. *Science* 327 (5970), 1246–1250. doi:10.1126/science.1182221

Shoji, H., Minami, H., Hachikubo, A., Sakagami, H., Hyakutake, K., Soloviev, V., et al. (2005). Hydrate-Bearing Structures in the Sea of Okhotsk. *Eos Trans. AGU* 86 (2), 13–18. doi:10.1029/2005EO020001

Sivan, O., Adler, M., Pearson, A., Gelman, F., Bar-Or, I., John, S. G., et al. (2011). Geochemical Evidence for Iron-Mediated Anaerobic Oxidation of Methane. *Limnol. Oceanogr.* 56 (4), 1536–1544. doi:10.4319/lo.2011.56.4.1536

Sivan, O., Schrag, D. P., and Murray, R. W. (2007). Rates of Methanogenesis and Methanotrophy in Deep-Sea Sediments. *Geobiology* 5 (2), 141–151. doi:10.1111/j.1472-4669.2007.00098.x

Skarke, A., Ruppel, C., Kodis, M., Brothers, D., and Lobecker, E. (2014). Widespread Methane Leakage from the Sea Floor on the Northern US Atlantic Margin. *Nat. Geosci.* 7 (9), 657–661. doi:10.1038/ngeo2232

Solomon, E. A., Kastner, M., MacDonald, I. R., and Leifer, I. (2009). Considerable Methane Fluxes to the Atmosphere from Hydrocarbon Seeps in the Gulf of Mexico. *Nat. Geosci.* 2, 561–565. doi:10.1038/ngeo574

Sommer, S., Linke, P., Pfannkuche, O., Niemann, H., and Treude, T. (2010). Benthic Respiration in a Seep Habitat Dominated by Dense Beds of Ampharetid Polychaetes at the Hikurangi Margin (New Zealand). *Mar. Geology.* 272 (1-4), 223–232. doi:10.1016/j.margeo.2009.06.003

Sommer, S., Linke, P., Pfannkuche, O., Schleicher, T., Schneider, D., Reitz, A., et al. (2009). Seabed Methane Emissions and the Habitat of Frenulate Tubeworms on the Captain Arutyunov Mud Volcano (Gulf of Cadiz). *Mar. Ecol. Prog. Ser.* 382, 69–86. doi:10.3354/meps07956

Sommer, S., Pfannkuche, O., Linke, P., Luff, R., Greinert, J., Drews, M., et al. (2006a). Efficiency of the Benthic Filter: Biological Control of the Emission of Dissolved Methane from Sediments Containing Shallow Gas Hydrates at Hydrate Ridge. *Glob. Biogeochem. Cycles* 20, a–n. doi:10.1029/2004GB002389

Sommer, S., Pfannkuche, O., Linke, P., Luff, R., Greinert, J., Drews, M., et al. (2006b). Efficiency of the Benthic Filter: Biological Control of the Emission of Dissolved Methane from Sediments Containing Shallow Gas Hydrates at Hydrate Ridge. *Glob. Biogeochem. Cycles.* 20 (2), GB2019. doi:10.1029/2004gb002389

Sommer, S., Türk, M., Kriwanek, S., and Pfannkuche, O. (2008). Gas Exchange System for Extended *In Situ* Benthic Chamber Flux Measurements Under Controlled Oxygen Conditions: First Application-Sea Bed Methane Emission Measurements at Captain Arutyunov Mud Volcano. *Limnol. Oceanogr. Methods.* 6 (1), 23–33. doi:10.4319/lom.2008.6.23

Somov, A., Baranov, A., Spirjakin, D., Spirjakin, A., Sleptsov, V., and Passerone, R. (2013). Deployment and Evaluation of a Wireless Sensor Network for Methane Leak Detection. *Sensors Actuators A: Phys.* 202, 217–225. doi:10.1016/j.sna.2012.11.047

Steinle, L., Graves, C. A., Treude, T., Ferré, B., Biastoch, A., Bussmann, I., et al. (2015). Water Column Methanotrophy Controlled by a Rapid Oceanographic Switch. *Nat. Geosci.* 8 (5), 378–382. doi:10.1038/ngeo2420

Stoll, H. M., and Bains, S. (2003). Coccolith Sr/Ca Records of Productivity during the Paleocene-Eocene thermal Maximum from the Weddell Sea. *Paleoceanography* 18 (2), a–n. doi:10.1029/2002PA000875

Suess, E., Torres, M., Bohrmann, G., Collier, R., Greinert, J., Linke, P., et al. (1999). Gas Hydrate Destabilization: Enhanced Dewatering, Benthic Material Turnover and Large Methane Plumes at the Cascadia Convergent Margin. *Earth Planet. Sci. Lett.* 170 (1-2), 1–15. doi:10.1016/S0012-821X(99)00092-8

Thomsen, T. R., Finster, K., and Ramsing, N. B. (2001). Biogeochemical and Molecular Signatures of Anaerobic Methane Oxidation in a marine Sediment. *Appl. Environ. Microbiol.* 67 (4), 1646–1656. doi:10.1128/AEM.67.4.1646-1656.2001

Torres, M. E., McManus, J., Hammond, D., De Angelis, M., Heeschen, K., Colbert, S., et al. (2002). Fluid and Chemical Fluxes in and Out of Sediments Hosting Methane Hydrate Deposits on Hydrate Ridge, OR, I: Hydrological Provinces. *Earth Planet. Sci. Lett.* 201 (3-4), 525–540. doi:10.1016/S0012-821X(02)00733-1

Tréhu, A. M., Flemings, P. B., Bangs, N. L., Chevallier, J., Gràcia, E., Johnson, J. E., et al. (2004). Feeding Methane Vents and Gas Hydrate Deposits at South Hydrate Ridge. *Geophys. Res. Lett.* 31 (23). doi:10.1029/2004GL021286

Treude, T., Boetius, A., Knittel, K., Wallmann, K., and Barker Jørgensen, B. (2003). Anaerobic Oxidation of Methane above Gas Hydrates at Hydrate Ridge, NE Pacific Ocean. *Mar. Ecol. Prog. Ser.* 264, 1–14. doi:10.3354/meps264001

Tromp, T. K., Van Cappellen, P., and Key, R. M. (1995). A Global Model for the Early Diagenesis of Organic Carbon and Organic Phosphorus in Marine Sediments. *Geochimica et Cosmochimica Acta.* 59 (7), 1259–1284. doi:10.1016/0016-7037(95)00042-X

Ussler, W., III, and Paull, C. K. (2008). Rates of Anaerobic Oxidation of Methane and Authigenic Carbonate Mineralization in Methane-Rich Deep-Sea Sediments Inferred from Models and Geochemical Profiles. *Earth Planet. Sci. Lett.* 266 (3-4), 271–287. doi:10.1016/j.epsl.2007.10.056

Valentine, D. L., Kessler, J. D., Redmond, M. C., Mendes, S. D., Heintz, M. B., Farwell, C., et al. (2010). Propane Respiration Jump-Starts Microbial Response to a Deep Oil Spill. *Science* 330 (6001), 208–211. doi:10.1126/science.1196830

Van Cappellen, P., and Gaillard, J.-F. (1996). Biogeochemical Dynamics in Aquatic Sediments. *Biogeochem. Dyn. Aquat. sediments. Reactive transport porous media.*, 335–376. doi:10.1515/9781501509797-011

Van Rensbergen, P., De Batist, M., Klerkx, J., Hus, R., Poort, J., Vanneste, M., et al. (2002). Sublacustrine Mud Volcanoes and Methane Seeps Caused by Dissociation of Gas Hydrates in Lake Baikal. *Geology* 30 (7), 631–634. doi:10.1130/0091-7613(2002)030<0631:smvams>2.0.co;2

van Kessel, T. G., Ramachandran, M., Klein, L. J., Nair, D., Hinds, N., Hamann, H., et al. (2018). Methane Leak Detection and Localization Using Wireless Sensor Networks for Remote Oil and Gas Operations. *IEEE SENSORS*, 1–4. doi:10.1109/icsens.2018.8589585

Veloso-Alarcón, M. E., Jansson, P., De Batist, M., Minshull, T. A., Westbrook, G. K., Pälike, H., et al. (2019). Variability of Acoustically Evidenced Methane Bubble Emissions Offshore Western Svalbard. *Geophys. Res. Lett.* 46 (15), 9072–9081. doi:10.1029/2019GL082750

von Deimling, J. S., Rehder, G., Greinert, J., McGinnnis, D. F., Boetius, A., and Linke, P. (2011). Quantification of Seep-Related Methane Gas Emissions at Tommeliten, North Sea. *Continental Shelf Res.* 31 (7-8), 867–878. doi:10.1016/j.csr.2011.02.012

Waage, M., Portnov, A., Serov, P., Bünz, S., Waghorn, K. A., Vadakkepuliyambatta, S., et al. (2019). Geological Controls on Fluid Flow and Gas Hydrate Pingo Development on the Barents Sea Margin. *Geochem. Geophys. Geosyst.* 20 (2), 630–650. doi:10.1029/2018GC007930

Wadham, J. L., Arndt, S., Tulaczyk, S., Stibal, M., Tranter, M., Telling, J., et al. (2012). Potential Methane Reservoirs beneath Antarctica. *Nature* 488, 633–637. doi:10.1038/nature11374

Wallmann, K., Aloisi, G., Haeckel, M., Obzhirov, A., Pavlova, G., and Tishchenko, P. (2006a). Kinetics of Organic Matter Degradation, Microbial Methane Generation, and Gas Hydrate Formation in Anoxic Marine Sediments. *Geochimica et Cosmochimica Acta* 70, 3905–3927. doi:10.1016/j.gca.2006.06.003

Wallmann, K., Drews, M., Aloisi, G., and Bohrmann, G. (2006b). Methane Discharge Into the Black Sea and the Global Ocean via Fluid Flow through Submarine Mud Volcanoes. *Earth Planet. Sci. Lett.* 248 (1-2), 545–560. doi:10.1016/j.epsl.2006.06.026

Wallmann, K., Drews, M., Aloisi, G., and Bohrmann, G. (2006c). Methane Discharge into the Black Sea and the Global Ocean via Fluid Flow Through Submarine Mud Volcanoes. *Earth Planet. Sci. Lett.* 248, 545–560. doi:10.1016/j.epsl.2006.06.026

Wallmann, K., Pinero, E., Burwicz, E., Haeckel, M., Hensen, C., Dale, A., et al. (2012). The Global Inventory of Methane Hydrate in Marine Sediments: A Theoretical Approach. *Energies* 5 (7), 2449–2498. doi:10.3390/en5072449

Wanninkhof, R. (1992). Relationship between Wind Speed and Gas Exchange Over the Ocean. *J. Geophys. Res.* 97 (C5), 7373–7382. doi:10.1029/92JC00188

Weber, T. C., Mayer, L., Jerram, K., Beaudoin, J., Rzhanov, Y., and Lovalvo, D. (2014). Acoustic Estimates of Methane Gas Flux from the Seabed in a 6000 Km^2 region in the Northern Gulf of Mexico. *Geochem. Geophys. Geosyst.* 15 (5), 1911–1925. doi:10.1002/2014GC005271

Wehrmann, L. M., Arndt, S., März, C., Ferdelman, T. G., and Brunner, B. (2013). The Evolution of Early Diagenetic Signals in Bering Sea Subseafloor Sediments in Response to Varying Organic Carbon Deposition over the Last 4.3Ma. *Geochimica et Cosmochimica Acta.* 109, 175–196. doi:10.1016/j.gca.2013.01.025

Wei, J., Wu, T., Deng, X., Haider, S. W., Kahkashan, S., and Yang, S. (2021). Seafloor Methane Emission on the Makran continental Margin. *Sci. Total Environ.* 801, 149772. doi:10.1016/j.scitotenv.2021.149772

White, R. S. (1979). Gas Hydrate Layers Trapping Free Gas in the Gulf of Oman. *Earth Planet. Sci. Lett.* 42 (1), 114–120. doi:10.1016/0012-821X(79)90196-1

Whiticar, M. J. (1999). Carbon and Hydrogen Isotope Systematics of Bacterial Formation and Oxidation of Methane. *Chem. Geology.* 161 (1-3), 291–314. doi:10.1016/S0009-2541(99)00092-3

Xu, W., and Germanovich, L. N. (2006). Excess Pore Pressure Resulting from Methane Hydrate Dissociation in marine Sediments: A Theoretical Approach. *J. Geophys. Res.* 111 (B1), 111. doi:10.1029/2004JB003600

Yamamoto, S., Alcauskas, J. B., and Crozier, T. E. (1976). Solubility of Methane in Distilled Water and Seawater. *J. Chem. Eng. Data.* 21 (1), 78–80. doi:10.1021/je60068a029

Yamazaki, T., Nakano, Y., Monoe, D., Oomi, T., Nakata, K., and Fukushima, T. (2006). "A Model Analysis of Methane Plume Behavior in an Ocean Water Column," in The Sixteenth International Offshore and Polar Engineering Conference: OnePetro).

Yun, T. S., Lee, C., Lee, J.-S., Bahk, J. J., and Santamarina, J. C. (2011). A Pressure Core Based Characterization of Hydrate-Bearing Sediments in the Ulleung Basin, Sea of Japan (East Sea). *J. Geophys. Res.* 116 (B2), B02204. doi:10.1029/2010JB007468

Zabel, M., and Schulz, H. D. (2001). Importance of Submarine Landslides for Non-steady State Conditions in Pore Water Systems—Lower Zaire (Congo) Deep-Sea Fan. *Mar. Geology.* 176 (1-4), 87–99. doi:10.1016/S0025-3227(01)00164-5

Zeebe, R. E. (2007). Modeling CO_2 Chemistry, $\delta^{13}C$, and Oxidation of Organic Carbon and Methane in Sediment Porewater: Implications for Paleo-Proxies in Benthic Foraminifera. *Geochimica et Cosmochimica Acta.* 71 (13), 3238–3256. doi:10.1016/j.gca.2007.05.004

Zhang, X., Du, Z., Luan, Z., Wang, X., Xi, S., Wang, B., et al. (2017). *In Situ* Raman Detection of Gas Hydrates Exposed on the Seafloor of the South China Sea. *Geochem. Geophys. Geosyst.* 18 (10), 3700–3713. doi:10.1002/2017GC006987

Conflict of Interest: The authors declare that the research was conducted in the absence of any commercial or financial relationships that could be construed as a potential conflict of interest.

Publisher's Note: All claims expressed in this article are solely those of the authors and do not necessarily represent those of their affiliated organizations, or those of the publisher, the editors and the reviewers. Any product that may be evaluated in this article, or claim that may be made by its manufacturer, is not guaranteed or endorsed by the publisher.